Properties of the First Genetically Engineered Neuron

Thesis by Hsiaolan S. Hsu

In Partial Fulfillment of the Requirements

for the Degree of

Doctor of Philosophy

California Institute of Technology

Pasadena, California

1993

(Submitted May 5th, 1993)

Acknowledgments

I would like to thank my advisor , Dr. H. A. Lester for his continuous support, academically and financially throughout my graduate career. I thank Dr. N. Davidson for his ongoing questions and attention. I thank Drs. X.C. Yang, B. Ho and C. Labarca for their invaluable help on the numerous technical twists and turns of my thesis project. I thank Dr. Labarca for constructing and supplying the pTM1NaIIA plasmid, graduate student A. Figl for subcloning the pTM1-KH4 plasmid, E. Huang for simulations of the Na^+ plateau, C. Nolan for preparing the cultured cells and growing virus and everybody in the Lester/Davidson lab for just being there.

I thank Drs. O. Elroy-Stein and B. Moss for furnishing vTF7-3, pTM1 and pTM1LacZ and for many helpful discussions, and Dr. C. Miller for the H4 plasmid and O. Bernander, F. A. Dodge, Jr., G. Laurent and C. Koch for discussions.

I would like to especially thank Drs. Nancy and Peter Lim for their friendship and generous support. I thank Dr. Chong Chen my husband for making my daily life exciting and eventful but often difficult and exhausting. I thank my mother-in-law and my parents for taking care of my son Byron, who makes everything worthwhile.

Abstract

Electrically excitable channels were expressed in Chinese hamster ovary cells using a vaccinia virus vector system. In cells expressing rat brain IIA Na^+ channels, brief pulses (< 1 ms) of depolarizing current resulted in action potentials with a prolonged (0.5 - 3 s) depolarizing plateau; this plateau was caused by slow and incomplete Na^+ channel inactivation. In cells expressing both Na^+ and *Drosophila* Shaker H4 transient K^+ channels, there were neuron-like action potentials. In cells with appropriate Na^+/K^+ current ratios, maintained stimulation produced repetitive firing over a 10-fold range of frequencies but eventually led to "lockup" of the potential at a positive value after several seconds of stimulation; the latter effect was due primarily to slow inactivation of the K^+ currents. Numerical simulations of modified Hodgkin-Huxley equations describing these currents, using parameters from voltage-clamp kinetics studied in the same cells, accounted for most features of the voltage trajectories. The present study shows that insights into the mechanisms for generating action potentials and trains of action potentials in real excitable cells can be obtained from the analysis of synthetic excitable cells that express a controlled repertoire of ion channels. This model system provides a direct control of complexity of neuronal behavior, and a tool for studying various forms of neural modulation at molecular and cellular levels.

Contents

List of Figures:

Chapter Two:

Chapter Three:

Chapter Four:

List of Tables

Chapter One
Introduction

The nervous system is one of the most complex biological systems. The elementary unit of the nervous system is a single neuron whose electrical activity underlies such cognitive functions as vision, motor control or learning. Precise pattern of neuronal excitability is generated by membrane proteins that are responsive to internal and external cues. At single cell level basic electrical activity varies from a single impulse to a complex burst of spikes. The actual waveform of an action potential affects information processing of the system.

Hodgkin and Huxley (1952) demonstrated elegantly the underlying ionic composition of an action potential. Their approach to the study of neuronal excitability consists of selective pharmacological activation or elimination of one particular ionic component, voltage clamp analysis of the kinetic properties of each ionic current, and numerical modeling of the action potential based on these experimentally derived kinetic properties. These methods have been proven to be tremendously powerful and successful, and are still primary ways to study the complexity of neural integration. It is known that neuronal activity is generated from interactions among numerous voltage-gated and ligand-gated ion channels, as well as receptors coupled to intracellular messengers. Modulation of channel activity by intracellular messengers can further modify the dynamics of neuronal excitability. However, these classical methods cannot always resolve the important functions of an individual component. For instance, the large potassium channel gene family lacks

specific pharmacological agents that can act on individual members. Furthermore, voltage-clamp analysis often cannot clearly separate the different potassium currents present in a neuron because some types are activated and inactivated at similar voltages. New methods would be helpful in the study of neuronal excitability.

To study interaction among ion channel proteins and their role in shaping neuronal behavior, we construct an artificial neuron which uses heterologous expression techniques to insert cloned neuronal ion channels into the cell membrane of a previously non-excitable cell. Instead of painstakingly teasing the various components of a neuron apart, we put them together one at a time. This new approach has two advantages. First, the system is well defined. We know exactly the composition of our artificial neuron. Second, the system can be easily manipulated. In combination with the tools of molecular biology, we hope to study in future questions such as the function of diverse potassium channels, the role of calcium channels in bursts of electrical activity, and the functional significance of channel modulation by phosphorylation.

Our strategy is first to demonstrate the validity of using artificial neurons to understand neuronal integration, and then combine this approach with computational methods to tackle more complex and unsettled issues. As a first step, we reconstitute the elementary activity of a neuron, namely an action potential, in a non-excitable cell. Generation of an action potential requires at least the presence of sodium and some type of potassium channels. Of numerous cloned Na^+ channel genes, we chose the rat brain type II sodium channel because it has been extensively studied and hence is well characterized physiologically, structurally and biochemically. For the potassium channel we chose the *Drosophila* Shaker potassium channel, the first potassium channel cloned, for similar reasons. When these two channels were expressed in non-

excitable Chinese hamster ovary (CHO) cells, the cells were able to generate single action potentials and trains of impulses whose frequency depended on the strength of stimulation. We expect that the behavior of the artificial neuron could be predicted from numerical simulations of the known channel kinetics. However, except for predicting the required Na^+ and K^+ channel densities, many properties of the artificial neuron were not predicted. Firing frequencies of the artificial neuron ranging from 1 to 20 Hz, were almost an order of magnitude lower than the initial simulated data. To explain this inconsistency, we systematically studied and characterized a slow component of Na^+ and K^+ currents. Although the slow and incomplete inactivation of Na^+ and K^+ channels has been documented in the literature, this property has not been systematically studied and its physiological function remains unknown. We found that these slow kinetics indeed critically determined the firing properties of the artificial neuron.

Without the artificial neuron approach, the functional significance of slow and incomplete inactivation of Na^+ and K^+ currents may not have been appreciated. And the role of sustained potassium current in maintaining the stability of neurons in general would not be found. Hence, we find that this approach not only was satisfactory in meeting our initial goals but also offered new insights to existing questions.

Chapter Two
The Vaccinia Virus Expression System

Introduction

Vaccinia virus is a member of poxvirus family that includes the deadly smallpox and cowpox viruses. Poxviruses, the largest of all animal viruses are about 200 to 400 nanometers (nm) long. Unlike other DNA viruses, they replicate in the cytoplasm of infected cells. These viruses are antigenically related and have similar morphology and vertebrate host range.

The genome of vaccinia virus is contained in a linear double-stranded DNA molecule of 187 kilobases (kb) pairs (Moss and Fexner, 1987). This DNA is packaged within the virus core, which also contains a complete transcription system. A viral-specific RNA polymerase, and all necessary post-transcriptional modifying enzymes ensure vaccinia a productive cytoplasmic life. Once vaccinia virus has entered the cell, its viral transcription system is activated and early genes are expressed within 6 hours. Early viral mRNAs are translated into proteins on cellular ribosomes soon after their transcription by viral enzymes. These early enzymes start replication and transcription of the viral DNA. Replication then signals the onset of expression of late genes which encode the majority of structural proteins assembled into virus particles. When complete vaccinia viral particles are assembled, most are retained inside the host cell. Only a small percentage of them are extruded into the extracellular space. This amount of extruded viral particles can vary from 1% to 30% depending on the strain of vaccinia virus and cell type (Moss, 1985).

The vaccinia virus expression system uses the ability of the virus to carry genes into a host cell and express them in the host cell environment. It is one of a few heterologous expression systems used for expressing integral membrane proteins, particularly mammalian genes. The other most commonly used eukaryotic expression systems are the microinjection of cDNA or mRNA into Xenopus oocytes, transient or stable transfection of mammalian cell lines, and the use of retrovirus and baculovirus.

The vaccinia virus expression system has several advantages compared to other expression techniques. First, it has an extraordinarily wide host range including mammals, birds and insects. Second, its infection rate is close to 100%. Third, its large genome can accommodate 25 kb of foreign DNA with no adverse effect on viral yield (Smith and Moss, 1983). An upper limit on the size of foreign DNA has not been demonstrated. Fourth, unlike other DNA viruses, its replication cycle resides in the cytoplasm of host cells. Thus synthesis of foreign proteins is controlled by viral enzymes and bypasses transcriptional regulation and RNA processing of the host cell nucleus. Expression using this method demonstrates reliable post-translational modification and targeted transport, such as insertion of integral membrane proteins into the appropriate apical or basolateral surface of epithelial cells (Stephens et al., 1986). Fifth, recombinant virus has been engineered with significantly reduced virulence.

However, the vaccinia virus system has its limitations. The virus kills the host cells within one week. The plasmid vector, named pTM1 (Figure 2) was constructed for efficient expression with vaccinia, but it is difficult to manipulate. Also, in my experience, the expression efficiency is inconsistent. It varies from less than 10% to 100% .

Construction of Recombinant Viruses

Homologous recombination is the standard technology for insertion of foreign DNA into nonessential regions of the vaccinia virus genome (Figure 1). The level of foreign gene expression depends on the transcriptional regulatory elements directly upstream from the start codon. Plasmid vectors that greatly facilitate insertion and expression of foreign genes possess a vaccinia transcription promoter and several restriction endonuclease sites (polylinker) for insertion of the foreign coding sequence, flanked by DNA from a nonessential region of the vaccinia genome. The most widely used vaccinia promoter, P7.5, contains both early and late signals that lead to continuous expression for 1-2 days. The flanking vaccinia DNA sequence determines the site of homologous recombination with the viral genome.

The formation of a recombinant virus relies on the spontaneous recombination rate that is less than 0.1%. The standard selection procedure utilizes the nonessential vaccinia virus thymidine kinase (TK) gene as a flanking sequence. Insertion of the foreign gene into the TK locus inactivates that gene. Selection of TK^- virus is carried out with a virus plaque assay in TK^- cells in culture in the presence of a nucleoside analog 5-bromodeoxyuridine (BrdU). Cells infected with TK^+ viruses are killed because phosphorylation of BrdU by the expressed thymidine kinase and subsequent incorporation into cellular DNA is lethal. Depending on the efficiency of the transfection (cellular uptake of plasmid vectors) and recombination, up to 80% of the plaques are desired recombinants and the rest are spontaneous TK^- mutants. These spontaneous TK^- mutants are then eliminated through several rounds of plaque hybridization that yield pure recombinant viruses.

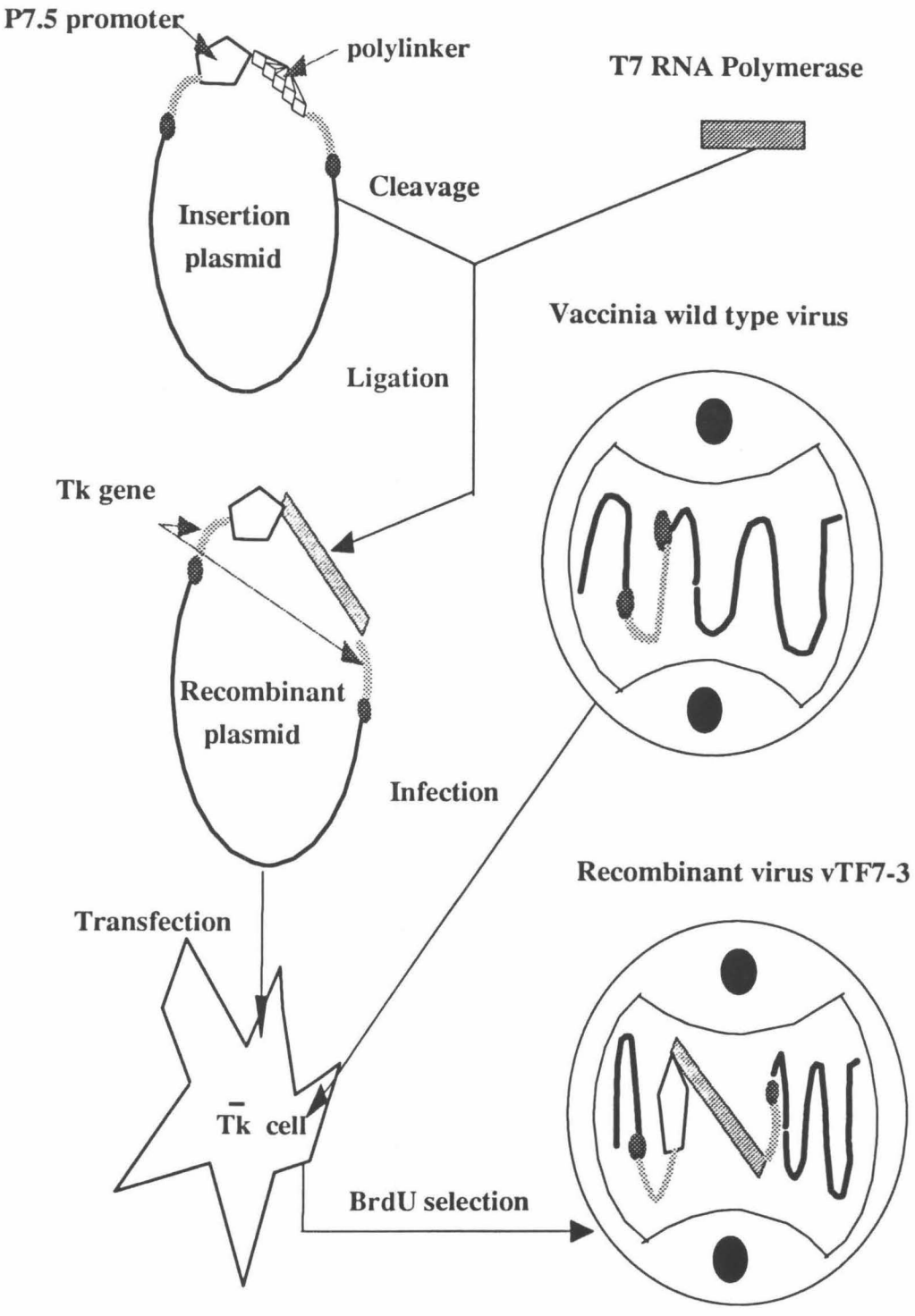

Figure 1. Construction of the Recombinant Virus, vTF7-3.

Figure 1. Construction of the Recombinant Virus, vTF7-3

Three major steps are involved in the construction of a recombinant virus. First, the gene of interest, in this case T7 RNA polymerase, is inserted into the insertion plasmid that contains the viral TK gene flanking sequence, P7.5 viral promoter and a polylinker. The new plasmid that carries the T7 RNA polymerase is called the recombinant plasmid. Second, TK^- cells which lack the TK gene are infected with the vaccinia wild-type virus and transfected with the recombinant plasmid. Spontaneous recombination in the TK genes of the recombinant plasmid and the wild-type virus produce a new type of virus that incorporates the T7 RNA polymerase into its genome. The final step is the BrdU selection, isolation and amplification of this recombinant virus. TK^- cells containing wild-type virus are killed by BrdU selection. The remaining survivors contain the recombinant virus vTF7-3 that has the T7 RNA polymerase incorporated into its genome.

Vaccinia Virus / T7 System

The vaccinia virus/T7 (VV/T7) hybrid expression system incorporates the highly efficient bacteriophage T7 RNA polymerase into the vaccinia virus system. The T7 RNA polymerase gene is integrated into the genome of vaccinia virus as outlined above (Figure 1). In the recombinant virus vTF7-3, the T7 RNA polymerase is under the control of the vaccinia promoter P7.5. Host cells are first infected with vTF7-3 and then transfected with a plasmid vector that encodes a reporter gene, β-galactosidase flanked by T7 promoter and terminator signals. Expression of the virus-directed T7 polymerase which recognizes the T7 promoter and terminator signals, leads to efficient transcription of this reporter gene. With this infection/transfection procedure, heterologous expression of β-galactosidase (β-gal) produced roughly 300 times more protein than simple infection with a recombinant virus containing the β-gal gene, and the percentage of cells expressing the recombinant protein also increased (Fuerst et al, 1986). These improvements are crucial to electrophysiologists who do single cell assays.

Further improvement of the system was spurred by the finding that only 5% of mRNAs transcribed by T7 RNA polymerase were capped and methylated. Because capping is required for efficient translation of mRNA in eukaryotic cells, protein synthesis from uncapped mRNA is limited. Inserting the encephalomyocarditis virus (EMCV) untranslated region (UTR), just downstream of the T7 promoter, facilitates cap-independent ribosome binding and increases protein production 5- to 10-fold (Elroy-Stein et al, 1989). The plasmid vector pTM1 combines the T7 promoter and EMCV UTR with only a *NcoI* restriction site at the polylinker (Figure 2). Placing the start codon of the insert at the *NcoI* site provides a consensus sequence for initiation

of translation. Unfortunately, the requirement that genes be placed immediatedly downstream of the EMCV UTR at the *NcoI* site makes insertion of cDNAs into pTM1 difficult.

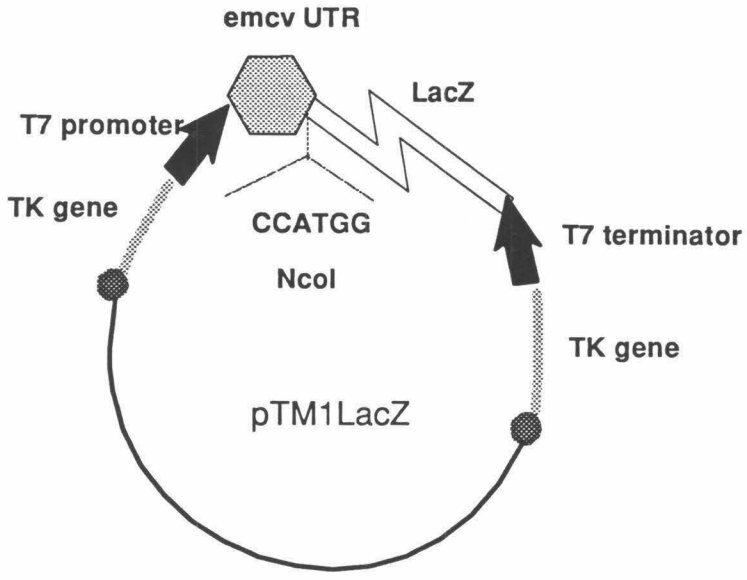

Figure 2. Schematic Diagram of Plasmid pTM1LacZ. The plasmid pTM1LacZ contains the TK gene flanking regions, T7 promoter and terminator sequences, and the EMCV UTR sequence upstream from the LacZ gene. LacZ encodes the E.coli β-galactosidase. EMCV UTR promotes efficient translation of the LacZ mRNA into protein.

Viruses and Plasmids

The two vaccinia recombinant viruses, vTF7-3 and VV:H4 encode the bacteriophage T7 RNA polymerase and the *Drosophila* Shaker H4 K^+ channel cDNAs respectively (Fuerst et al, 1986; Elroy-Stein et al, 1989; Leonard et al, 1989). Both viruses are under the control of the vaccinia promoter P7.5. Na^+ and K^+ channel cDNAs were inserted into the plasmid pTM1 downstream from the T7 promoter, T7 hairpin, and encephalomyocarditis virus 5' untranslated region (Figure 3A). Construction and expression of the Na^+ channel plasmid, pTM1-NaIIA, has been described by Yang et al (1992). The cDNA encoded leu at position 860. The Shaker H4 cDNA was furnished by M. Tanouye and mutated by Klaiber et al (1990) to provide an *Nco*I site at the initial ATG codon. The *Nco*I/*Eco*RI fragment was excised from pBluescript (Stratagene), transferred to pTM1, and named pTM1KH4.

Expression

Figure 3 illustrates two alternative methods used in our studies for heterologous expression of ion channels using vaccinia virus. In the first, CHO cells were infected with vTF7-3 and transfected with pTM1NaIIA and pTM1KH4 (Figure 3A). T7 polymerase expressed from the recombinant virus transcribes the Na^+ and K^+ channel genes, and the host cell machinery completes translation of the mRNA and incorporation into the plasma membrane. Occasionally, only one plasmid was used to express either the Na^+ or K^+ channel alone. In the second method, CHO cells were infected with vTF7-3 and VV:H4 and transfected with pTM1NaIIA (Figure 3B). T7 polymerase in this case transcribes the Na^+ channel gene only and VV:H4 expresses the K^+ channel gene.

CHO cells were plated on 35-mm dishes. 16-20 h later, cells were rinsed with phosphate-buffered saline containing 1 mM $MgCl_2$ (PBS-M) containing 0.1% bovine serum albumin and were infected with vTF7-3 at a multiplicity of infection (MOI) of 10 for 30-35 min. Cells were then exposed to serum-free culture medium (α-MEM plus 100 units/ml penicillin, 100 units/ml streptomycin, 2 mM glutamate, non-essential amino acids) plus DNA-Lipofectin complex (Bethesda Research Labs) and incubated for 24 h. Concentrations of pTM1NaIIA plasmid DNA, pTM1KH4 plasmid DNA, and Lipofectin were respectively, 3.2 μg, 0.4 μg, and 9.6 μg. The DNA-Lipofectin complex was formed by mixing plasmid DNA with Lipofection and incubating for 20 min at room temperature. Cells were then maintained in culture medium plus 5% bovine serum albumin.

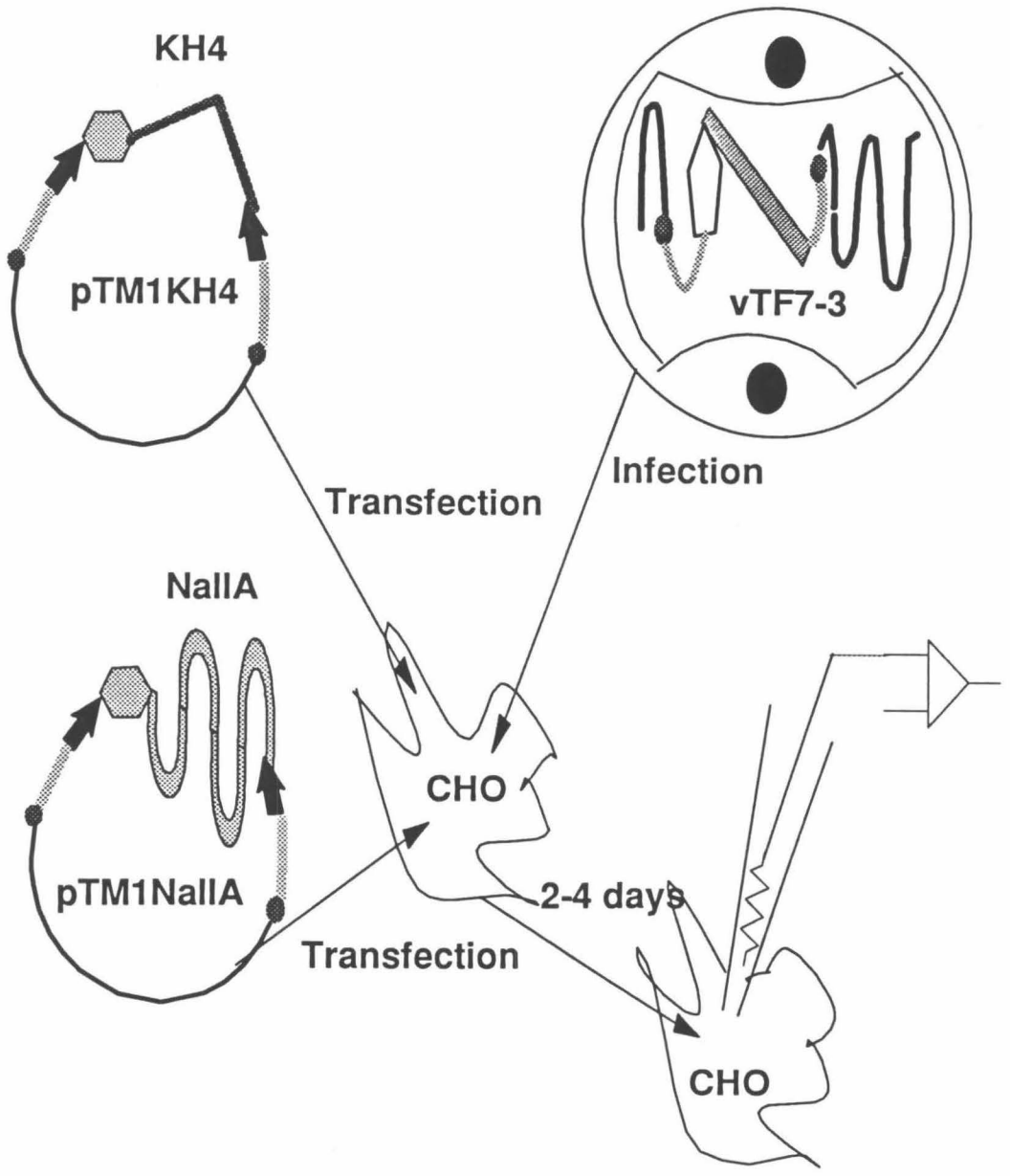

Figure 3A. Protocol for Expression of Na^+ and K^+ Channels with the Vaccinia / T7 Hybrid Expression System.

CHO cells were first infected with vTF7-3 and transfected with pTM1KH4 and pTM1NaIIA. Two to four days after this infection and transfection procedure, CHO cells were recorded with an electrode to study the expressed Na^+ and K^+ channels

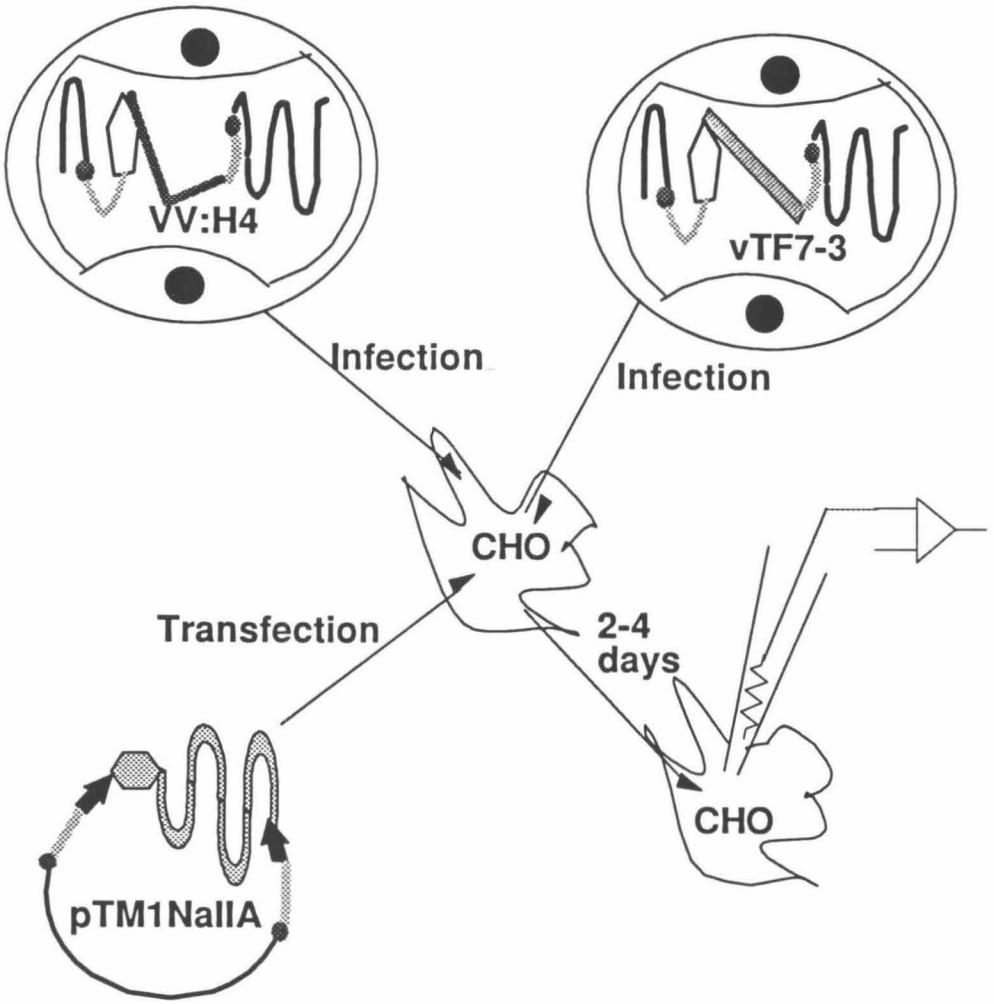

Figure 3B. Protocol for Expression of Na^+ Channel with the Vaccinia / T7 Hybrid Expression System and K^+ Channel with Only Vaccinia Virus Expression.

CHO cells were infected with VV:H4 and vTF7-3 and transfected with pTM1NaIIA. Two to four days after the infection and transfection procedure, CHO cells were recorded with an electrode to study the expressed Na^+ and K^+ channels.

Efficiency of Na^+ and K^+ Channel Expression

The combination of vaccinia virus and T7 RNA polymerase expression system (VV/T7) and pTM1 was known to significantly increase the expression efficiency for soluble proteins (i.e., expression of β-gal discussed above). However the same result has not been shown for integral membrane proteins. We therefore compared expression of the Shaker K channel using VV:H4 infection and that obtained with the VV/T7 system. The K^+ channel gene is under the control of the P7.5 viral promoter in the recombinant virus VV:H4, but is under the control of the T7 promoter in the plasmid pTM1KH4. As an internal control in both types of experiments, we used the VV/T7 system to express Na^+ channels. Table I compares the channel expression efficiency obtained with pTM1NaIIA, pTM1KH4, and vTF7-3 (abbreviated T7 system) to that obtained with pTM1NaIIA, vTF7-3 and VV:H4 (abbreviated VV system). The data on Na^+ channel expression showed that the internal control worked well. Expression efficiencies of Na^+ channel are similar in both methods. The data on K^+ channel expression (bold numbers) showed that the T7 promoter is superior to the endogenous viral promoter not only for soluble proteins but also for integral membrane proteins. Undoubtedly this fact is responsible for the increased efficiency of expression for both Na^+ and K^+ channels and the decreased failure rate. Therefore the results in Chapter 3 were obtained using the VV/T7 system to express Na^+ and K^+ channels.

TABLE 1. EXPRESSION EFFICIENCY FOR Na^+ AND K^+ CHANNELS

Expression System	Na^+ channel	K^+ channel	Na^+ & K^+ channels	Failure
T7	0.33 ± 0.02	**0.52** ± 0.04	0.25 ± 0.02	0.40 ± 0.03
(n)	(48)	(43)	(33)	(39)
VV	0.28 ± 0.04	**0.19** ± 0.03	0.12 ± 0.03	0.65 ±0.06
(n)	(22)	(22)	(17)	(50)

Expression of Na^+ and K^+ channels were assayed electrophysiologically. The total numbers of recorded whole cells for T7 and VV are 940 and 366, respectively. The entries are given in mean ± sem of (n) separate studies. The expression efficiency is calculated by dividing the number of positive cells by the total of number of recorded cells in each study. Failure is the percentage of non-expressing cells.

To further optimize VV/T7 expression system, the multiplicity of infection (MOI) for vTF7-3 was varied from 5 to 30 in increments of 5. MOI of 10-20 gave the best result. For MOI higher than 20, cell death rate was significantly increased. Next, concentrations in μg per 35mm dish of pTM1KH4 and pTM1NaIIA were varied (see details in Methods). The optimal plasmid DNA concentrations are 5 μl/dish for Na^+ channels and 2-2.5 μg/dish for K^+ channels (Table II). Thus, under optimal conditions, the probability of expressing both Na^+ and K^+ channels could be above 50%. However, the general requirement for making repetitive firing cells (details in Chapter 3) is that Na^+ current must be larger than K^+ current in a given cell. More than 1 μg/dish of pTM1KH4 in all cases produced K^+ current larger than the Na^+ current and hence non-repetitive firing cells. To obtain repetitive firing cells, I used 0.4-0.5 μg/dish of pTM1KH4 and 3.0-4.0 μg/dish of pTM1NaIIA for the experiments discussed in Chapter 3.

TABLE 2. EFFECT OF PLASMID CONCENTRATIONS ON EXPRESSION EFFICIENCY IN VV/T7 SYSTEM

pTM1KH4 (μg/dish)	Efficiency (n)	pTM1NaIIA (μg/dish)	Efficiency (n)
0.04 - 0.1 (n)	0.34 (161)	2.0 - 2.5	0.21 (42)
0.20 - 0.25	0.36 (126)	3.0 - 3.2	0.30 (221)
0.4 - 0.5	0.44 (234)	4.0	0.32 (461)
0.8	0.36 (44)	**5.0**	**0.47** (38)
1.0 - 1.2	0.63 (116)	6.0	0.32 (72)
2.0 - 2.5	**0.72** (32)		
4.0 - 8.0	0.43 (33)		

Tests designed to optimize the DNA-Lipofectin ratio in the transfection steps did not yield any quantitative results. The general findings are 1) Lipofectin alone kills the CHO cells, contradictory to the manufacturer's report; 2) mortality rate of cells transfected with a DNA-Lipofectin ratio of less than 1:6 was 90%, even without viral infection; 3) more than 20 μg/dish of Lipofectin reduced input resistance (R_{in}) of whole cell recordings to one-tenth that of normal cells (Lipofectin ≤ 13 μg/dish).

LacZ staining (see Appendix 1) was used as a qualitative assay for the transfection/infection procedure. Since LacZ staining results were usually obtained 4 hours after the procedure and one day before electrical recordings, a quantitative relationship between β-galactosidase expression and channel expression facilitate electrophysiology experiments. In Figure 5 the percentage of cells expressing, either Na^+ or K^+ channels are plotted against the percentage of β-galactosidase positive cells for 12 experiments. Slope and intercept of the regression line are 0.27 and 41% with a correlation coefficient of 0.38. This low correlation coefficient indicated in general that LacZ staining is not a quantitative indicator of the channel expression level.

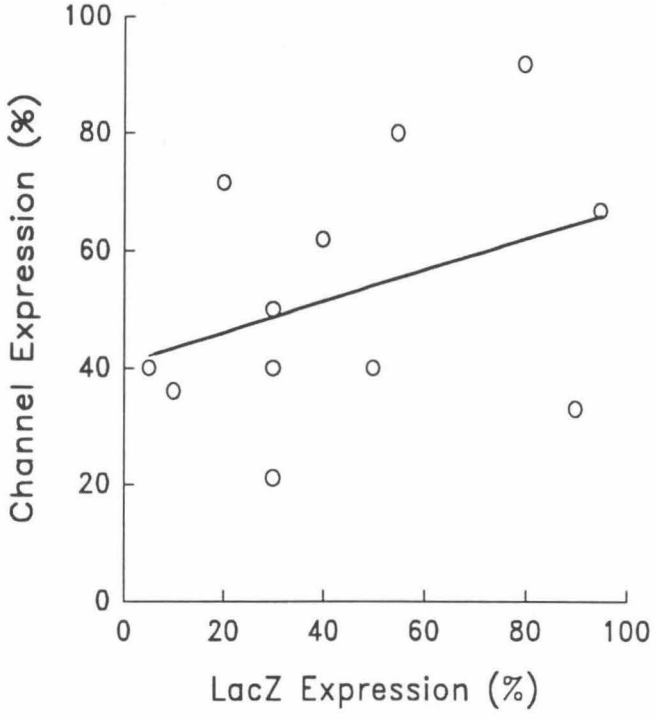

Figure 4. Correlation of LacZ and Channel Expressions.

Channel expression is only loosely correlated with LacZ expression.

Chapter Three
Properties of the Artificial Neuron

Introduction

The electrical and chemical excitability of neurons is controlled by a large repertoire of membrane proteins, including ion channels activated by changes in potential, channels activated by extracellular and intracellular ligands, 7-helix receptors coupled to G proteins, transporters, and ion pumps. These excitability proteins allow neurons to generate series of nerve impulses whose temporal pattern reflects various stimuli and modulatory influences. At present, several major approaches are available to analyze the contribution of a particular channel, receptor, or transporter to impulse firing patterns: (*1*) pharmacological activation and elimination, (*2*) antisense suppression of a particular protein, and (*3*) numerical modeling based on channel gating kinetics. We introduce an additional approach based on heterologous expression of foreign excitability proteins, in this case voltage-dependent channels. We contend that the new approach aids in hypothesis testing and enables the construction of entirely new classes of excitable cells.

A minimum requirement for the generation of a neuron-like action potential (Hodgkin and Huxley, 1952) would be the presence of one Na^+ channel type and one K^+ channel type and a means to maintain an appropriate resting potential (a possible exception is provided at some node of Ranvier which lack K^+ channels). To estimate approximately the channel density required, we note that the Na^+ current should be

sufficient to charge the membrane capacitance [C = 0.01 pF/$(\mu m)^2$] to a supra-threshold depolarization ($\Delta V \sim 40$ mV) before the Na^+ channels inactivate ($\Delta t = 0.4$ ms). One therefore has $I = C\Delta V/\Delta t = 1$ pA/$(\mu m)^2$, corresponding to ~ 1 Na^+ channel/$(\mu m)^2$. Vaccinia virus (VV) expression systems are capable of expressing several channel types simultaneously at the required levels and were therefore employed (Leonard et al, 1989; Karschin et al, 1991a; Yang et al, 1992)

All-or-none action potentials were indeed recorded in these simple synthetic neurons. Interestingly, however, we have found that the encoding properties of these cells are more complex than would be expected simply on the basis of voltage-clamp data on the expressed Na^+ and K^+ currents on a millisecond time scale. Recent data emphasize that both endogenous and heterologously expressed mammalian Na^+ currents (Llinas, 1988; Krafte et al, 1988; Krafte et al, 1990; Zhou et al, 1991) and expressed *Drosophila* Shaker H4 currents (Iverson and Rudy 1990, Hoshi et al, 1991) display slow and incomplete inactivation on a time scale of seconds. In an iterative series of experiments involving electrophysiological measurements and numerical simulation, we found that these slow properties help to determine the voltage trajectories in the synthetic neurons. Slow inactivation of transient K^+ currents could play a role in the encoding properties of real neurons as well.

Electrophysiology

Culture dishes containing infected/transfected cells were rinsed twice with bath solution (145 mM NaCl, 5 mM KCl, 1.8 mM $CaCl_2$, 1.2 mM $MgCl_2$, 10 mM HEPES, pH 7.4). Patch pipettes were pulled from Sutter thick-walled glass tubing on a Sutter P-80 puller and filled with intracellular solution (120 mM KCl, 25 mM KCl, 5 mM NaCl, 1 mM $MgCl_2$, 10 mM HEPES, 5 mM EGTA, pH 7.2). Tip resistances were

2-5 MΩ. Recordings were performed with an Axopatch-1D (Axon Instruments, Foster City, CA) circuit under the control of pCLAMP software (Axon Instruments) running on MS-DOS computers. Tetrodotoxin (300 nM) was applied by pressure from the tip of a pipette positioned ~ 5 μm from the cell. Records shown are typical of at least 5 cells in each case.

Results

We employed cDNA clones for the rat brain IIA Na^+ channel (Auld et al, 1988a; Auld et al, 1990) and for the *Drosophila* Shaker H4 transient K^+ channel (Kamb et al, 1987; Iverson et al, 1988). To express the channels, cells were infected by a vaccinia virus expressing the bacteriophage T7 RNA polymerase and were also transfected by plasmids containing the channel cDNA downstream from the T7 promoter and the 5' untranslated region of the encephalomyocarditis virus (Elroy-Stein et al, 1989). Control ("mock transfection") experiments utilized identical virus and plasmid vectors, but the cDNA encoded β-galactosidase rather than a channel.

In voltage-clamp experiments, mock-transfected control cells displayed little or no voltage-dependent currents (Figure 5A). Cells transfected with either the Na^+ or K^+ channel plasmids displayed only Na^+ or K^+ currents, respectively (Figures. 5B, 5C), as expected from previous studies on expression using the highly efficient infection-transfection procedure (Yang et al, 1992) and related vaccinia expression systems (Leonard et al, 1989; Karschin et al, 1991a, b). Cells transfected with both the Na^+ and K^+ channel plasmids displayed both the inward and outward voltage-dependent currents appropriate to both channel types (Figure 5D). The peak current densities ranged from 100 to 450 pA/pF for Na^+ (at -10 mV) and from 100 to 700 pA/pF for K^+ (+50 mV). There are no detailed single-channel studies on these two channel types for the ionic concentrations used in our experiments; but previous measurements with oocyte expression lead one to estimate values of ~ 15 pS for both channel types (Iverson et al, 1988; Krafte et al, 1990). Therefore assuming that the cell membrane has a capacitance of 0.01 pf/μm^2 these whole-cell currents correspond to a channel density of 1.5 to 7 Na^+ channels/μm^2 and 0.6 to 4 K^+ channels/μm^2.

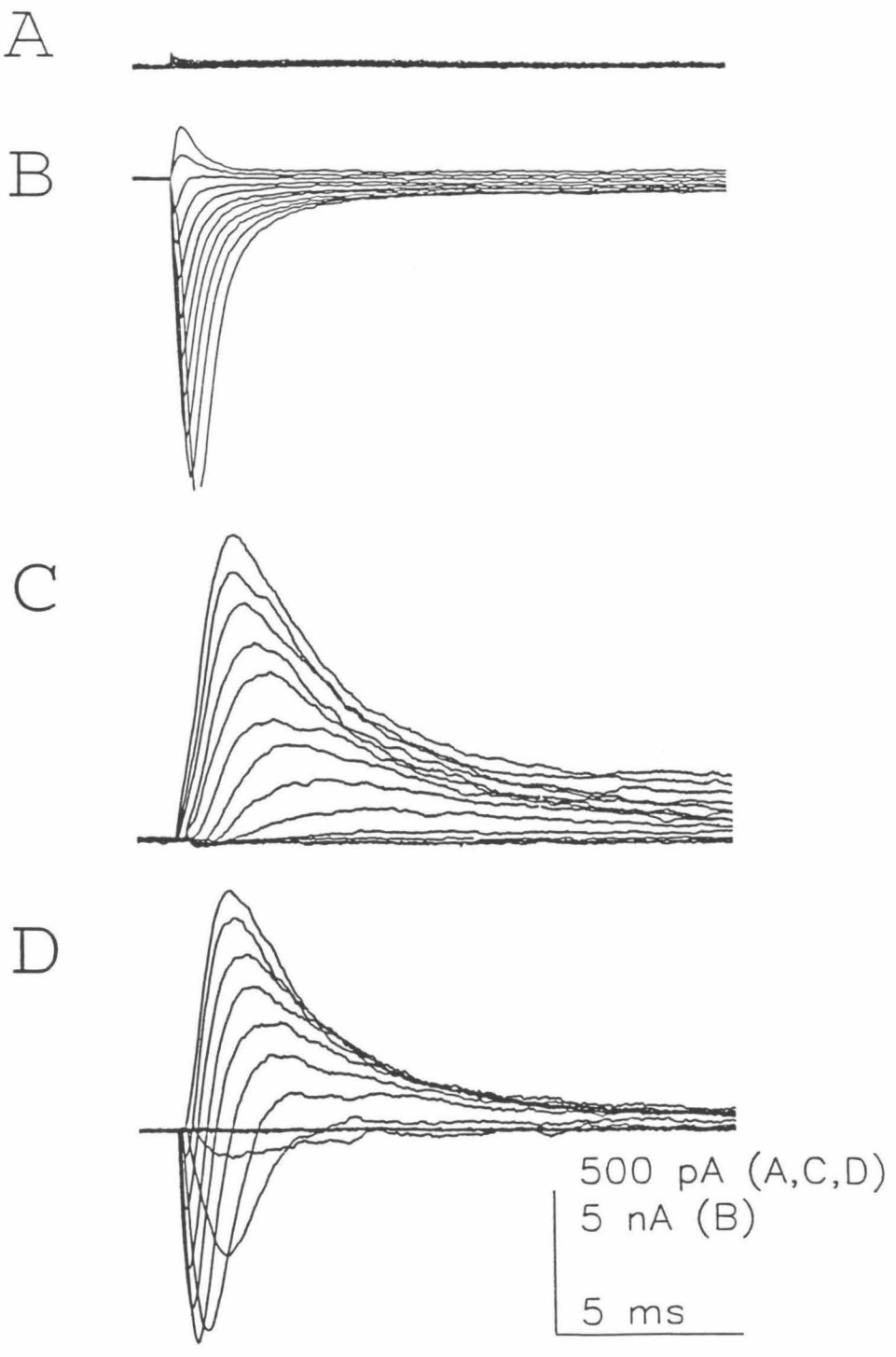

Figure 5 Voltage-Clamp Records on a Millisecond Time Scale

Figure 5 Voltage-Clamp Records on a Millisecond Time Scale.

Records from 4 different cells, illustrating the expression combinations used in these experiments. Each cell was infected with vTF7-3 and transfected with various plasmids based on pTM1. A, Control cell. Transfection with pTM1LacZ, encoding β-galactosidase. There are no voltage-dependent currents. B, Transfection with pTM1NaIIA, encoding the Na^+ channel. C, Transfection with pTM1KH4, encoding the K^+ channel. D, Transfection with both pTM1NaIIA and pTM1KH4. In A, C, and D, records were obtained with a holding potential of -70 mV and test potentials in 10 mV increments between -60 mV and +60 mV. In all panels, leakage currents have been subtracted off-line. In B, the presentation has been optimized to illustrate the small non-inactivating component of Na^+ current. Holding potential, -100 mV; test potentials at 10 mV increments between -20 mV and +80 mV. The peak currents were greater than 10 nA. These large currents vitiated high-fidelity voltage-clamp feedback and saturated the recording equipment. Particular attention was paid to determine the non-inactivating component, as follows. (1) Passive and capacitive components were subtracted on-line in a P/4 procedure. (2) A further off-line correction of 0.3 nS was required to produce zero current near the reversal potential (+65 mV); and this was subtracted from all the records.

The present analysis concerns data obtained when these cells were studied with current-clamp recording--a procedure that was the standard electrophysiological measurement for intracellular recording from neurons before patch techniques enabled high-fidelity voltage clamping. In current-clamp recording, the electronics are arranged so that the voltage trajectory is governed by the time-dependent gating of ionic channels as well as by the passive resistance and capacitance of the cell. This arrangement models the situation in a real neuron as it responds to synaptic stimuli from other cells.

Cells Expressing Na^+ Channels

Figure 6A illustrates the voltage trajectory in a cell subjected to a brief (0.5 ms) pulse of outward (depolarizing) current, superimposed on a steady hyperpolarizing current to maintain the membrane potential at a level more negative than -70 mV in order to eliminate Na^+ current inactivation. In nearly all cells studied, the response began with a rapid depolarization that approached the expected reversal potential for Na^+ channel currents, +65 to +75 mV. (This range is less positive than the Na^+ equilibrium potential, +85 mV, because the Na^+ channel has a finite permeability to K^+; see Hille, 1991).

The subsequent voltage trajectory did not resemble a neuronal action potential; instead, it resembled a cardiac action potential. A few ms after reaching its peak, the membrane potential became less positive, then remained at a depolarized plateau for a variable period of several hundred ms to several seconds (Fig. 6A, traces 1 through 5). In experiments with timed puffs of Tetrodotoxin, we showed that these plateaus depend directly on Na^+ channels rather than on any possible small

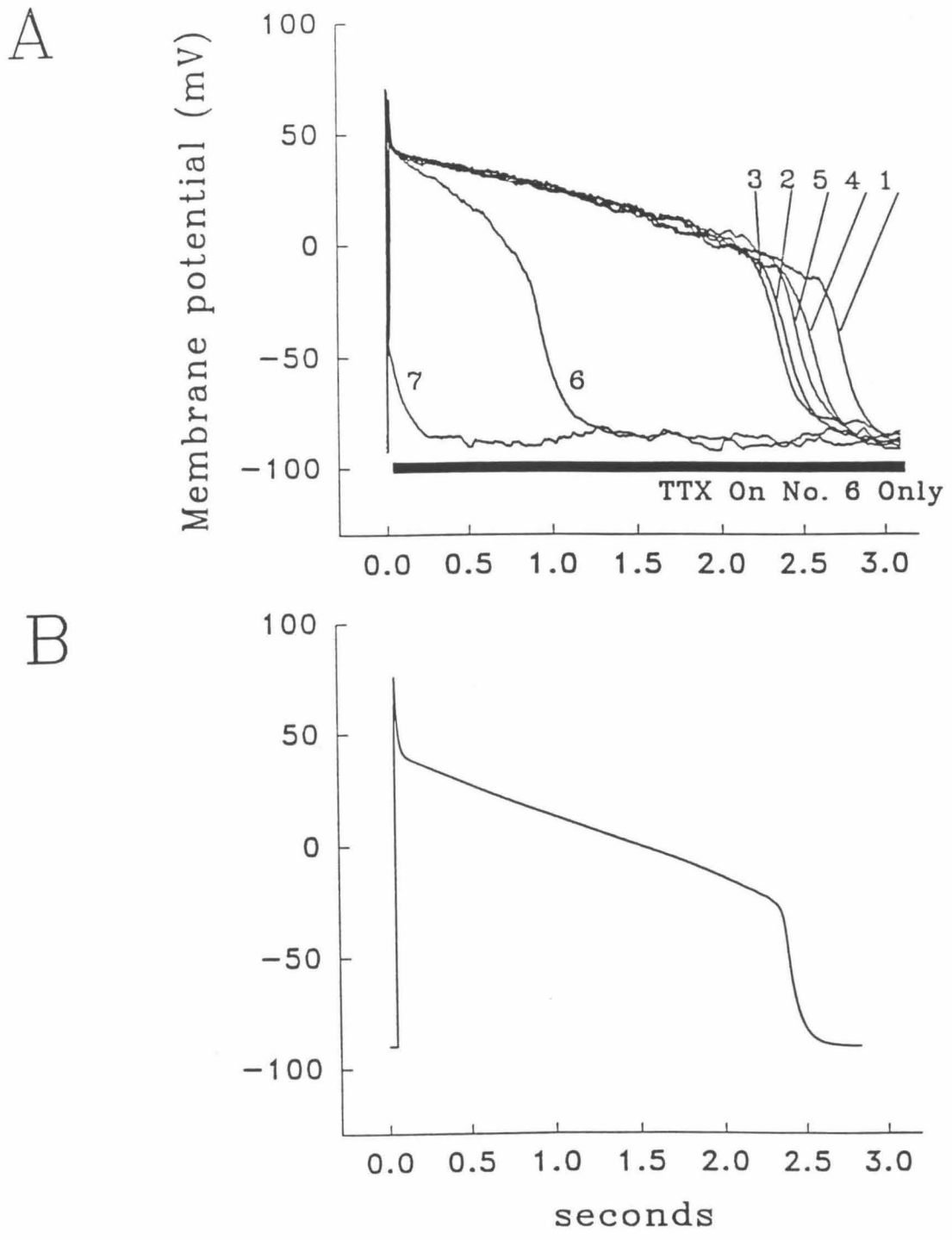

Figure 6. Analysis of the Heartlike Action Potentials in a Cell Expressing Only Na^+ Channels and an Unusually Prolonged Plateau.

Figure 6. Analysis of the Heartlike Action Potentials in a Cell Expressing Only Na^+ Channels and an Unusually Prolonged Plateau.

(A) Voltage recordings during a current-clamp experiment. The trial comprised 7 episodes, at intervals of 10 s. In each case, the action potential was evoked by a depolarizing pulse at time zero (0.5 ms, 0.7 nA, superimposed on a -20 pA steady current). During episode 6, TTX (300 nM) was applied from a puffer pipette for the period indicated by the bar. TTX application began 24 ms after the depolarizing pulse; therefore the early peak currents were not affected but the prolonged, small currents were blocked. The TTX pulse shortened the plateau, indicating that it is produced by the Na^+ channels. The Na^+ channels remained blocked during episode 7 but recovered over the next min (not shown). (B) Simulated plateau;

$\varepsilon_{Na} = 0.01$, $\tau_{2,Na,0} = 2000$ ms, $\bar{g}_{Na} = 47.5$ pS/μm^2, $\bar{g}_K = 0$; $\bar{g}_{leak} = 0.15$ pS/μm^2; these parameters are defined later in the text.

endogenous voltage-dependent properties that might have been overlooked in previous studies (Fig. 6A, traces 6 and 7). For further phenomenological analysis, we abstracted the parameters of the plateau as indicated in Table III. There was a noticeable effect of expression level on the duration of the plateau: for cells with average peak Na^+ currents of 2 nA, the plateau lasted < 1 s; for currents near 10 nA, the plateau lasted > 3 s. The variations among trials on the same cell (Fig. 6A) were probably caused by both (a) fluctuations in the seal resistance and (b) spontaneous fluctuations in the relatively small numbers of Na^+ channels open during the plateau.

Action potential waveforms with prolonged plateaus are typical of cardiac cells, such as Purkinje fibers and ventricular myocytes, and are rarely observed in neurons. However, in previous experiments where (a) only Na^+ channels were stimulated, (b) voltage-dependent K^+ channels were eliminated, and (c) resting conductances were very low, similar plateaus have been observed (Chandler and Meves, 1970d). The most likely reason for the plateau is that Na^+ channels do not inactivate completely. One source of incomplete Na^+ channel inactivation would be the "window" of overlay between steady-state activation and steady-state inactivation. For the IIA Na^+ channel expressed in CHO cells, this window occurs at -40 to -20 mV (Yang et al, 1992). (In the top panel of Figure 8A, which is described more completely below in connection with the simulations, the window is the region of overlap between the theoretical curves for h_∞ and for m_∞^3). Simulations confirmed that cells with the Na^+ current kinetics measured by Yang et al (1992) could produce plateaus in this window region of membrane potential. However, the average recorded plateau began at +21 mV and ended at -19 mV (Table III); these potentials

are much too positive to be consistent with the idea that "window current" causes the plateau.

Table III. Parameters of 12 plateaus in 5 cells expressing only Na^+ currents

Measured Parameter	Mean ± S.D.	Range	Simulated
Vstart (mV)	+21.7 ± 7.8	+37 to +12	+21
Vend (mV)	-19.2 ± 9.2	-34 to +3	-21
Vave (mV)	+3.7 ± 9.5	-10 to +21	-2
Duration (sec)	1.92 ± 0.91	0.54 to 3.1	1.9

The parameters were defined as follows. For each action potential, the slope was determined for the most slowly varying part of the trajectory; V_{start} and V_{end} were the potentials at which the slope increased by 5-fold. V_{ave} and duration were then defined over the interval between V_{start} and V_{end}. Parameters of the simulation are given in the text.

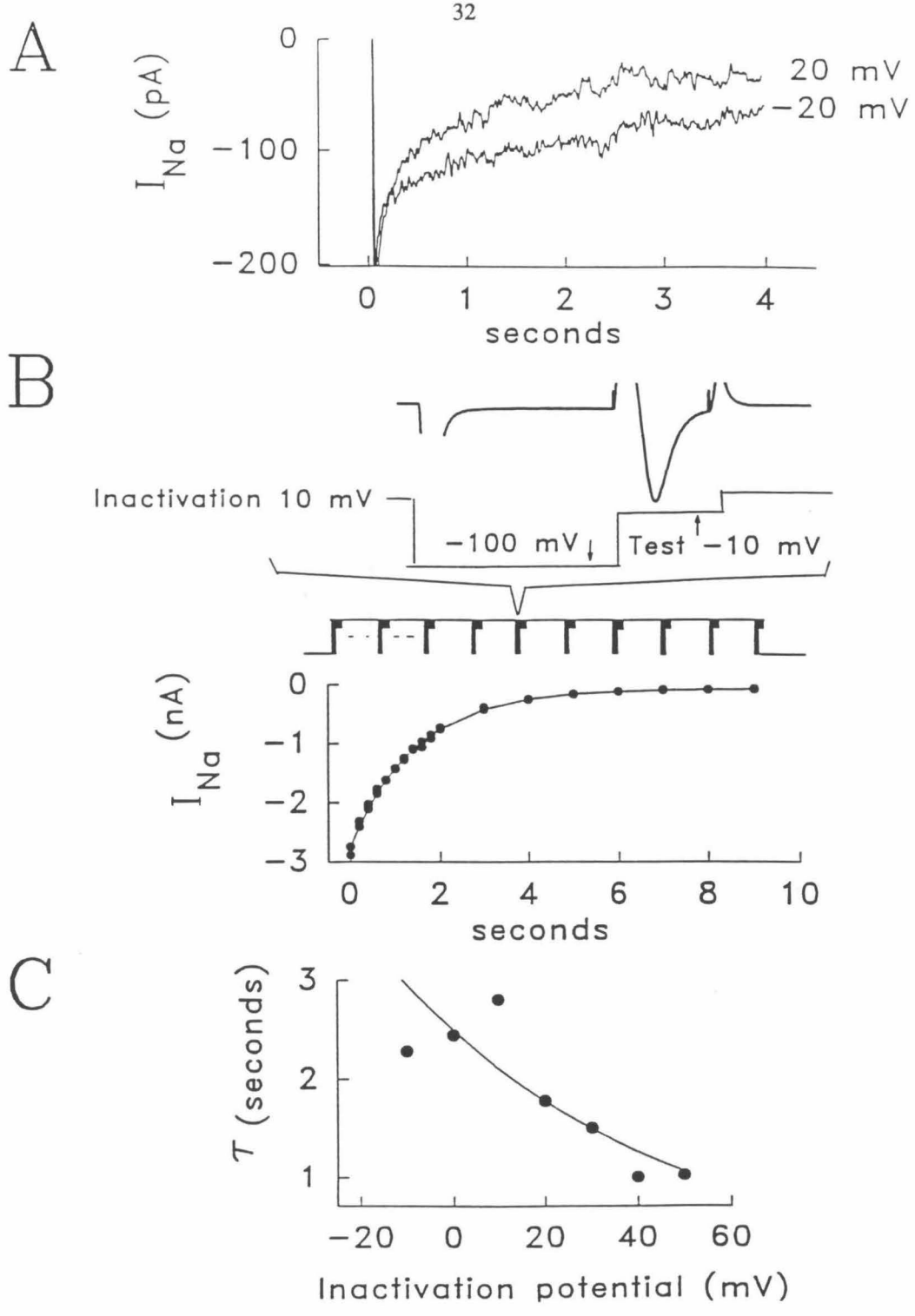

Figure 7. Current Recordings During Voltage-Clamp Analysis of a Slowly Inactivating Na^+ Current Component at Positive Potentials.

Figure 7. Current Recordings During Voltage-Clamp Analysis of a Slowly Inactivating Na^+ Current Component at Positive Potentials.

(A) Direct detection of slowly inactivating current. The holding potential was -100 mV and the test potentials are indicated. The early peaks of inward Na^+ are offscale and exceeded 10 nA. Episodes occurred at intervals of 10 s. A digital filter (10 ms) was applied to the data, and a linear 0.5 nS leak conductance has been digitally subtracted. (B) An example of voltage-clamp protocol and data for measuring Na^+ channel availability during inactivation. Before the trial, the holding potential was -100 mV. During the trial (10 s), the potential was usually held at the inactivating level (+10 mV in this example). At intervals of 200 ms, the potential was briefly (4.8 ms) returned to a reactivating level (-100 mV) to remove fast inactivation, briefly (2.4 ms) jumped to the test level (-10 mV) to assess Na^+ current availability, then returned to the inactivating level. Inactivation time constant is 1.5 s. (C) Slow inactivation time constants as a function of voltage for 5 cells, including that of (B). The line corresponds to an *e*-fold change for 60 mV.

Because our experiments were conducted in normal extracellular Na^+, the currents were sufficiently large to reveal an additional slowly inactivating component of Na^+ current not studied systematically in the experiments of Yang et al (1992), which were conducted with only 10 mM external Na^+. In Fig. 7B, for instance, roughly 1% of the peak Na^+ currents remain at the end of the 20 ms depolarizing pulses. Because apparent incomplete Na^+ inactivation could conceivably arise from incorrectly subtracted leakage currents, we used several different protocols to confirm the continued activation. The phenomenon was observed whether leak currents were subtracted by a P/4 procedure (each of 7 cells) or by Tetrodotoxin application (one cell).

Additional observations relevant to slow Na^+ inactivation are presented in Figure 7. In the experiment of Figure 7A, the cell was held at the hyperpolarized potential of -100 mV for 10s, then depolarized to the indicated test potential (+20 mV or -20 mV) for 4s. The very large initial current (> -10 nA) largely decayed in a few ms (fast inactivation) and is not shown; the figure shows the subsequent slow inactivation of the residual 1-2% of the current (records are typical of 4 cells). To confirm that these slow relaxations do not reflect other voltage-dependent conductances, we inverted the Na^+ concentration gradient by using 120 mM internal and 40 mM external Na^+. In each of 5 experiments, the slow relaxations were now outward at potentials between 0 and +40 mV (data not shown). The slowly inactivating currents were not large; at 100 ms, they averaged 1% to 3% of the peak value; but the data leave no doubt that maintained Na^+ conductances occur in these cells.

We found it most reliable to analyze the time course of slow inactivation by measuring Na^+ channel availability. This is the fraction of channels that can open

because they are not inactivated, during prolonged depolarizations (Figure 7B & 7C). After inactivation for a variable period at a given inactivation potential (+10 mV in Figure 7B), fast inactivation was removed with brief hyperpolarizing prepulses to -100 mV; and Na^+ currents were then measured during a 2.4 ms test pulse to -10 mV. These currents are plotted as a function of time at the inactivating potential in Figure 7B. When such data were fit to a single exponential, the time constants for decay were on the order of 0.5 to 3 s (1.5 s in Figure 7B), roughly appropriate to account for the duration of the plateau. We also found an intermediate component of inactivation with time constants on the order of several hundred ms; this component was not studied systematically.

Our experiments included numerical simulations of the voltage trajectories, as described in Chapter 4. We followed the usual practice of simulating the voltage trajectory for several exemplar cells (for instance, that of Figure 11) that yielded complete data; the parameters were then verified with data from the entire set of recorded cells. In such simulations, the Na^+ con ductance is usually described as $\bar{g}m^3h$, where $\bar{g}$ is the maximal Na^+ conductance (corresponding to simultaneous opening of all the Na^+ channels) and m and h (the activation and inactivation parameters, respectively) vary between 0 and 1. The variables m and h satisfy first-order differential equations that govern the voltage- and time-dependent behavior of the Na^+ conductance. The steady-state value for m is termed m_∞ and depends on potential, varying from 0 at potentials more negative than -40 mV to 1 at potentials more positive than 0 mV. The value for h_∞ varies in the opposite direction, form 1 at -60 mV to 0 at -20 mV. These steady states are approached exponentially with a voltage-dependent time constant τ; $\tau = 1/(\alpha + \beta)$, where α and β are the two voltage-dependent microscopic rate constants that govern partial steps in opening and closing

of the channel, respectively (discussed more fully in Hodgkin and Huxley, 1952). The equations are integrated numerically to describe how the Na^+ currents charge the equivalent circuit for the membrane, consisting of a capacitance in parallel with a passive conductance (Figure 17).

For the present work, we modified the $\bar{g}m^3h$ formalism to include two inactivation parameters *h1* (fast) and *h2* (slow). The modified term is $\bar{g}\,m^3[\varepsilon + h_1(1-\varepsilon)]h_2$. Other formalisms, for instance a simple addition of terms in $\bar{g}m^3h_1$ and $\bar{g}m^3h_2$, would also be acceptable; the present formalism was chosen because it served well for simulations of the K^+ conductance (see below). The parameter ε was less than 5% in our experiments and simulations; because h_1 decays essentially to zero over a few ms in the voltage range studied in Figure 6, the term in brackets above rapidly approaches the parameter ε which corresponds to the small fraction of current that inactivates with the slow time constant, $\tau_{h2,Na}$. A possible molecular interpretation of ε might be the fraction of time that channels spend in a non-inactivating state.

For Na^+ activation,

$$m_{\infty,Na} = \frac{1}{1+\exp\left(-\frac{V+28.7}{7}\right)};$$

$$\alpha = \frac{100}{10+\exp\left(-\frac{V-7}{8}\right)};$$

$$\beta = 0.01\exp\left(-\frac{V+50}{10}\right);$$

For Na^+ inactivation,

$$\varepsilon_{Na} = 0.02;$$

$$h_{1\infty,Na} = h_{2\infty,Na} = \frac{1}{1 + \exp\left(\frac{V + 40}{6}\right)};$$

$$\alpha = 0.0044 \exp\left(-\frac{V + 30}{9.5}\right);$$

$$\beta = \left[\frac{96}{1 + 0.087 \exp\left(\frac{V + 61}{5.7}\right)} + 1.2\right]^{-1};$$

$$\tau_{h2,Na} = 800 + \tau_{2,Na,0} \exp\left(-\frac{V}{60}\right); \qquad 750 \leq \tau_{2,Na,0} \leq 1500$$

where the voltages are in mV and the time constants are in ms. Parameters for ε_{Na} and $\tau_{h2,Na}$ were determined from experiments like those of Fig. 9B and C. $\tau_{h2,Na}$ is plotted vs. voltage in Figure 10A. Descriptions of $m_{\infty,Na}$, $\tau_{m,Na}$, and $h_{1\infty,Na} = h_{2\infty,Na}$ were taken from the work of Yang et al (1992) and also plotted in Figure 8A. The parameters given above yielded an adequate simulation of the average plateau summarized in Table III.

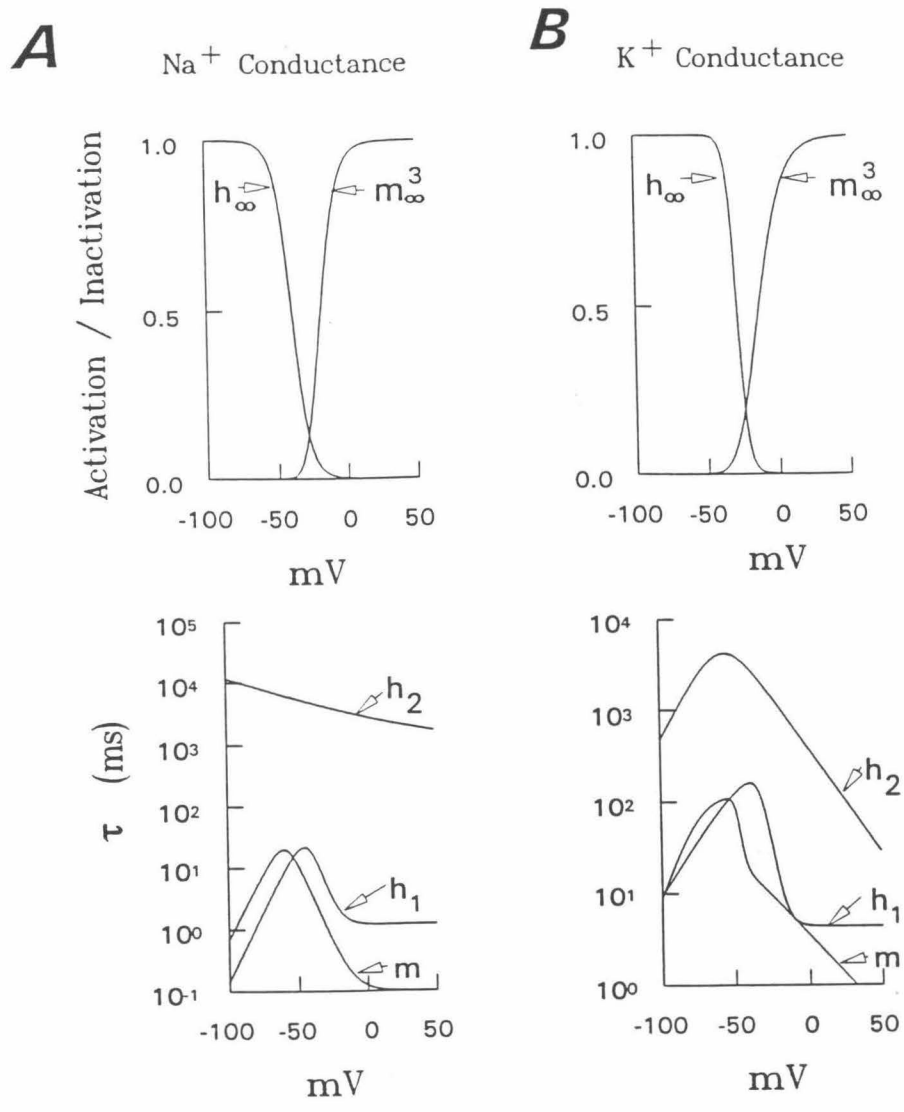

Figure 8. Voltage-Dependence of the Parameters Used in the Simulations, According to the Equations Given in the Text.

(A) parameters governing Na^+ conductance; (B) parameters governing K^+ conductance. Top panels give the equilibrium parameters m_∞, m_∞^3, and h_∞; bottom panels give the kinetic parameters τ_m, τ_{h1}, and τ_{h2}. the "window" of overlap between steady-state inactivation h_∞ occurs in the range -40 mV to -20 mV for Na^+ and -60 mV to -20 mV for K^+.

Cells Expressing K^+ Channels

In cells that were infected with the vaccinia virus vTF7-3 and transfected with the K^+ channel plasmid only (Fig. 7B), there were transient outward currents that strongly resembled those for Shaker H4 channels expressed in oocytes (Timpe et al, 1988a; Iverson et al, 1988) and in mammalian cells infected with a recombinant vaccinia virus encoding H4 directly (Leonard et al, 1989; Karschin et al, 1991a). In current-clamp mode with zero injected current, however, we noticed an additional phenomenon: the resting potentials were substantially more negative than for cells not expressing K^+ channels. In cells with peak K^+ currents greater than 1 nA at +50 mV, the average resting potential was -26.8 $\pm$ 2.6 mV (mean $\pm$ sem, n = 20), in contrast to values of -6.1 $\pm$ 1.1 mV (n = 34) for mock-transfected cells and -5.5 $\pm$ 1.6 mV (n = 11) for cells transfected with Na^+ channels only.

These more negative resting potentials can be explained by the presence of a steady K^+ conductance. This steady conductance would have escaped notice in earlier measurements on mammalian cells expressing K^+ channels; for instance, in a cell with an input resistance of 3 GΩ (a typical value in our mock-transfected cells), the steady conductance would correspond to an additional 0.1 nS, or a small fraction of the average 70 nS peak K^+ conductance at +50 mV, and could not decisively be distinguished from fluctuations in seal resistance. The important point for the present experiments, however, is that this steady K^+ conductance represents a component, due to Shaker channels, that inactivates either very slowly (> 10 min) or not at all.

Slow and incomplete inactivation of the Shaker H4 K^+ currents has also been observed by Iverson and Rudy (1990) and termed "C"-type inactivation in a detailed study (Hoshi et al, 1991). To provide the experimental data for quantitative

simulations of the voltage trajectories described below, we studied the inactivation of the K^+ currents over a wide time range. Figure 9A shows a protocol similar to that used in Figure 7A for Na^+ currents. When the voltage is jumped from a hyperpolarized holding potential of -100 mV, there is a rapid decay from the peak outward current greater than 10 nA; the behavior of the subsequent slowly inactivating component is shown. These slowly inactivating K^+ components were larger than the slowly inactivating Na^+ currents described above, ranging between 10% and 20% of the peak K^+ current. However, the crucial range for this study is -50 mV to -40 mV, which accounts for most of the voltage trajectory in a repetitively firing cell (see Figure 11A below). A protocol that measured K channel availability during prolonged depolarizations, similar to that used for Na^+ currents, was suitable for most of this voltage range (Figure 9B, 9C).

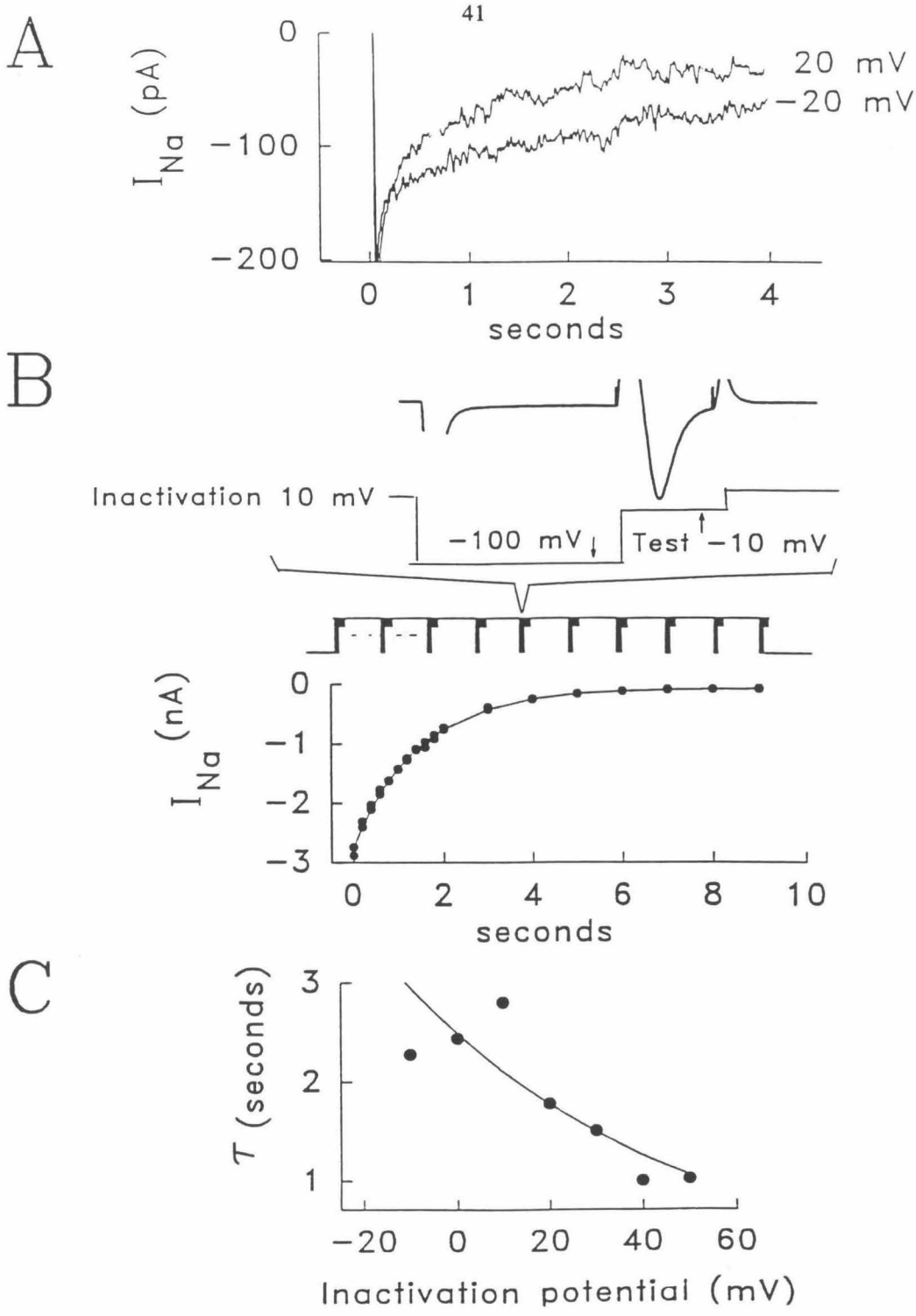

Figure 9. Voltage-Clamp Protocols and Data for Measuring Slow K^+ Channel Inactivation

Figure 9. Voltage-Clamp Protocols and Data for Measuring Slow K^+ Channel Inactivation

(A) Jumps to various test potentials at intervals of 25 mV from a holding potential of -100 mV; episodes at intervals of 10 s. The large early peaks of outward current (several nA) are off scale and have been cut off. (B) Data from a different cell, showing protocol and data from a trial with multiple episodes. There was a variable period at the inactivating potential (-10 mV in this example) followed by a test pulse to +50 mV to assess K^+ channel availability. Holding potential, -100 mV. The inactivation time constant is 1.78 s. (C) Voltage dependence of the time constants for the cell of B; smooth line shows an *e*-fold change for 15.5 mV.

Cells Expressing Both Na^+ and K^+ Channels

In current-clamp experiments on cells that expressed both channel types (Figure 10A), hyperpolarizing current pulses produced only passive voltage deflections with a time constant determined by the membrane resistance (3.3 ± 0.48 GW, mean ± sem for 43 cells; range 0.3 to 13.6 GW,) and capacitance (12.3 ± 1.33, range 8-20 pA). Likewise, subthreshold depolarizing currents produced only passive responses. For depolarizations to a threshold value that ranged from -15 to -50 mV (average value was -24.5 mV for 80 cells), the response was an all-or-none action potential with a classical waveform including a peak at +65 to +75 mV (the Nernst potential for Na^+) and, during maintained depolarizing currents, a brief hyperpolarizing undershoot. (Figures 10, 11A, and 12). The traces of Figure 10B, in which action potentials are elicited by a brief current pulse, demonstrate true regenerative behavior: the action potential does not require continued applied current once threshold is reached.

Previous results suggest that repetitive firing would be present in cells possessing transient voltage-dependent conductances for Na^+ and for K^+, if the Na^+ conductance is sufficiently large (Connor and Stevens, 1971a, b, c; H. Hsu, unpublished calculations). Of the 80 cells that produced action potentials in our study, ~ 20% displayed peak Na^+ to K^+ currents ratios of 2 or greater; and 8 of these cells yielded complete current- and voltage-clamp experiments. Each of these cells showed repetitive firing at stable frequencies for at least 8 impulses or 2 s (whichever came first) in response to maintained depolarizing currents (Figure 13). For these cells, the average ratio of peak Na^+ to K^+ currents was 2.01 and the spike threshold averaged -40 mV, versus 0.64 and -21 mV for cells that did not fire repetitively. Firing frequencies *f* were in the range 0.5 - 15 Hz in most cells (Figure 11A is an

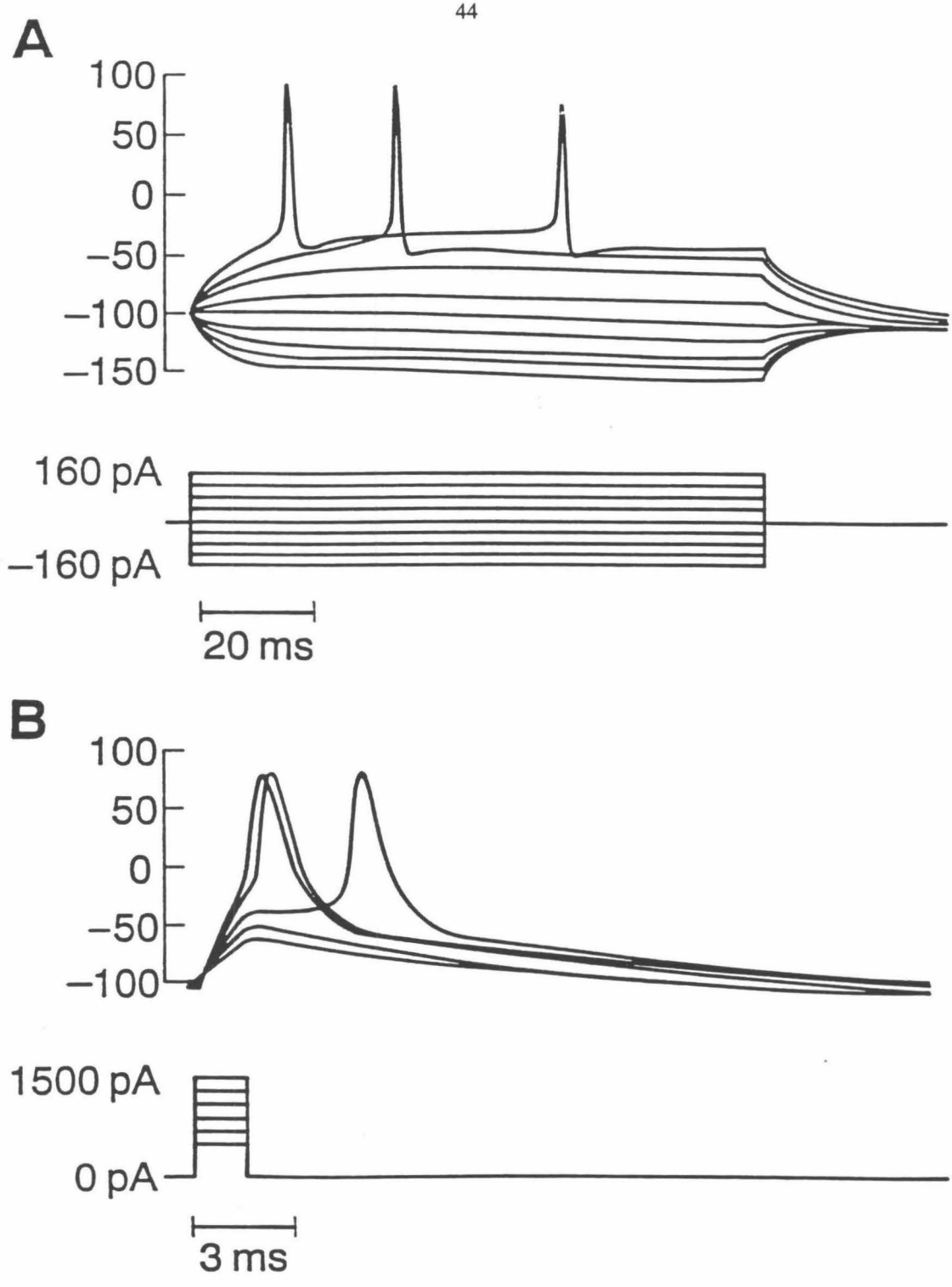

Figure 10. Neuronlike Action Potentials in Current-Clamp Recordings from Cells Expressing Both Na^+ and K^+ Channels.

Figure 10. Neuronlike Action Potentials in Current-Clamp Recordings from Cells Expressing Both Na^+ and K^+ Channels.

(A) Records during a series of 105-ms pulses ($\pm$40, $\pm$80, $\pm$120, and $\pm$160 pA from a holding current of -230 pA). The hyperpolarizing pulses produced only passive responses; the depolarizing pulses produced action potentials. (B) 1.5 ms pulses ranging in amplitude from 500 to 1500 pA from a holding value of -320 pA.

11A

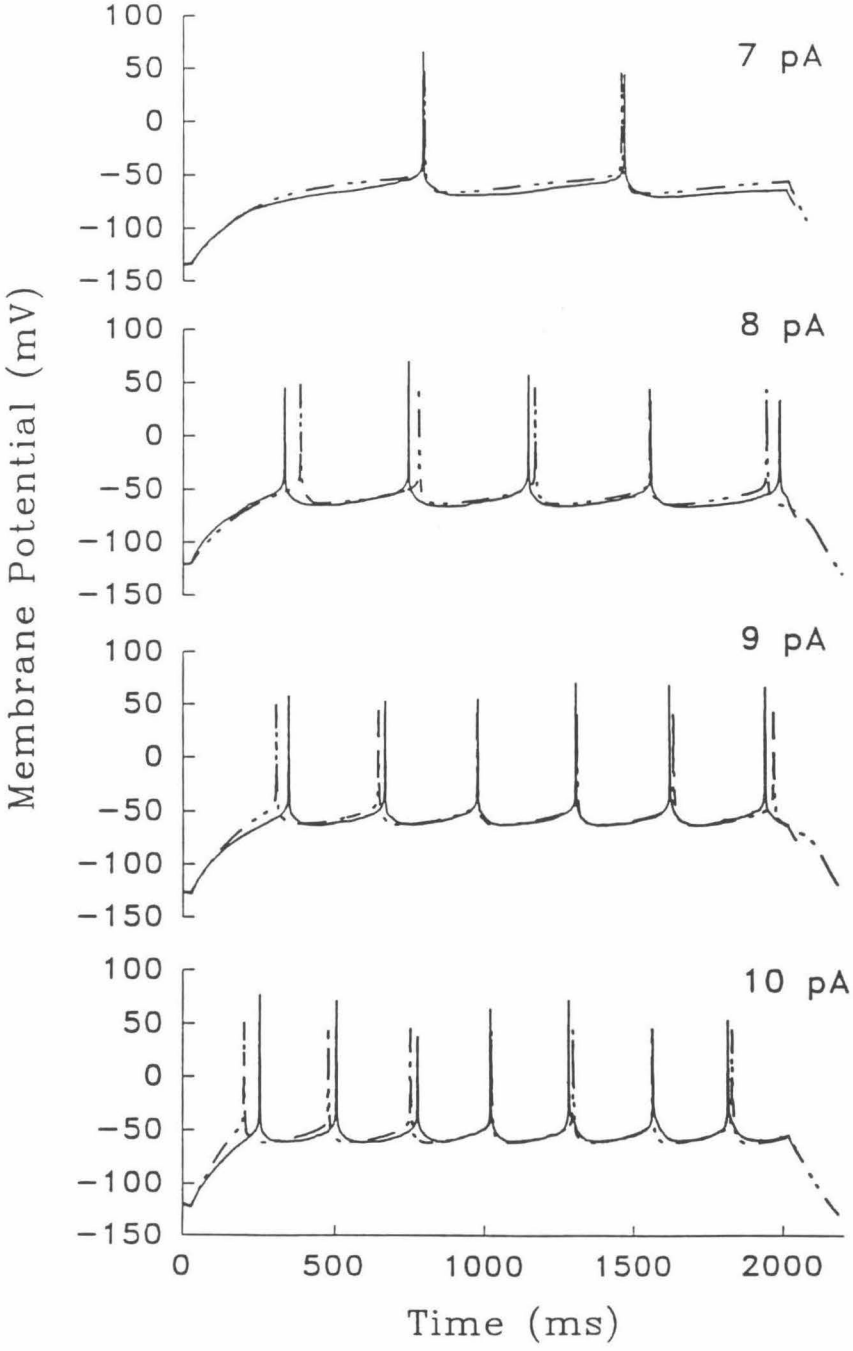

Figure 11A. Recorded and Simulated Voltage Trajectories from a Single Cell.

11B

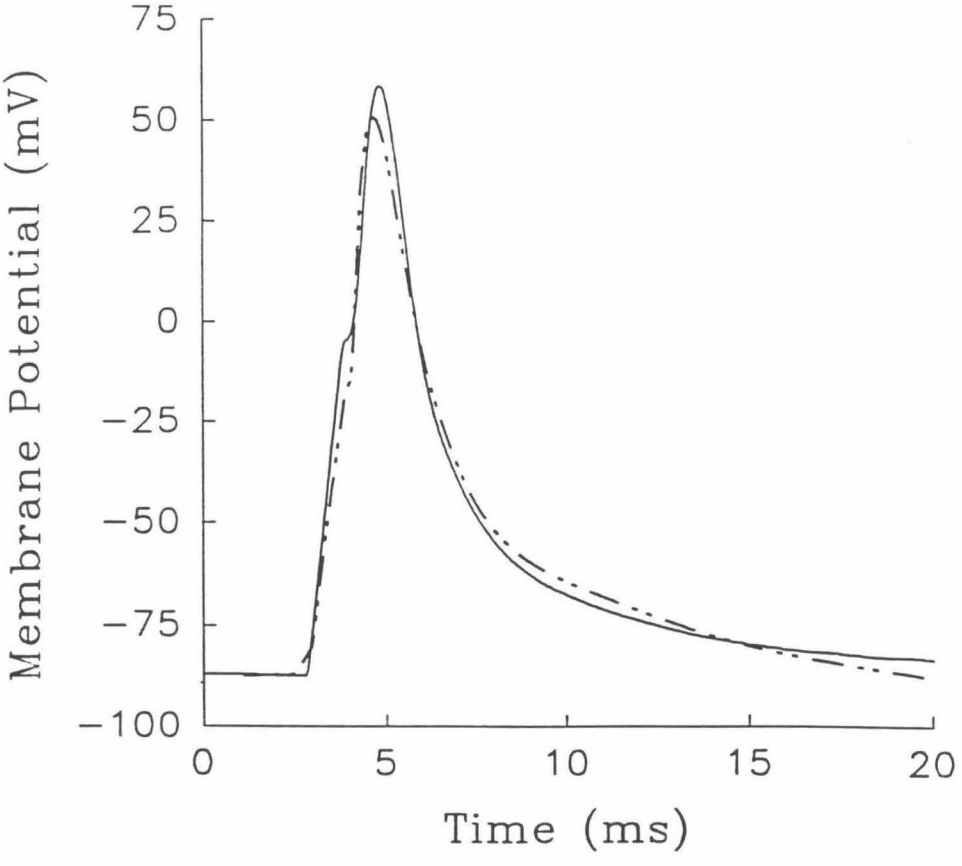

Figure 11. Recorded (Heavy Traces) and Simulated (Light Traces) Voltage Trajectories from a Single Cell.

(A) The holding current was -30 pA and the depolarizing currents were applied for 1.9 s at the indicated amplitudes. The peaks of the recorded spikes appear variable because of the low digitizing rate (1 kHz). (B) The holding current was -200 pA and the depolarizing current was applied for 1 ms at 1 nA.

example) and increased in a roughly linear fashion with stimulus current amplitude *I*. (This is illustrated in Figure 11A; Figure 19A shows a plot of *f* vs. *I* for the exemplar cell). The average constant of proportionality *f/I* was 0.43 ± 0.14 Hz/pA (mean ± sem). For the cells that fired repetitively, *f/I* did not depend strongly on the amplitudes of the Na^+ or K^+ conductances or on their ratios; we did however find that this parameter decreased with increasing cell capacitance (Figure 22).

We call attention to three interesting features of the impulse trains. (1) There was a wide frequency range. Firing rates covered at least a 10-fold range in each cell. (2) For large depolarizing currents, the potential became less negative during successive interspike intervals, as shown by the superpositions in Figure 12 B. Eventually the potential "locked up" at a value above 0 mV and no further impulses were obtained (Figures 12, and 14). "Lock-up" occurred at lower frequencies for cells with lower K^+ conductance. (3) Interspike intervals remained relatively constant during the depolarization, until "lockup" occurred (Figures 12A and 14).

These voltage trajectories were studied quantitatively with numerical simulation, as described below. However, we first present a qualitative overview of the features that seem to account for the "lock-up". A voltage-activated K^+ conductance, such as the Shaker H4 expressed in these cells, would be expected to terminate the action potential by repolarizing the cell and deactivating the Na^+ conductance. The gradually less negative potential during successive interspike intervals and eventual "lock-up" after several seconds would then result from the declining availability of these K^+ channels, due to slow inactivation. As noted above, appropriate slow inactivation of heterologously expressed Shaker H4 K^+ channels has been observed (Iverson and Rudy 1990; Hoshi et al, 1991) and termed

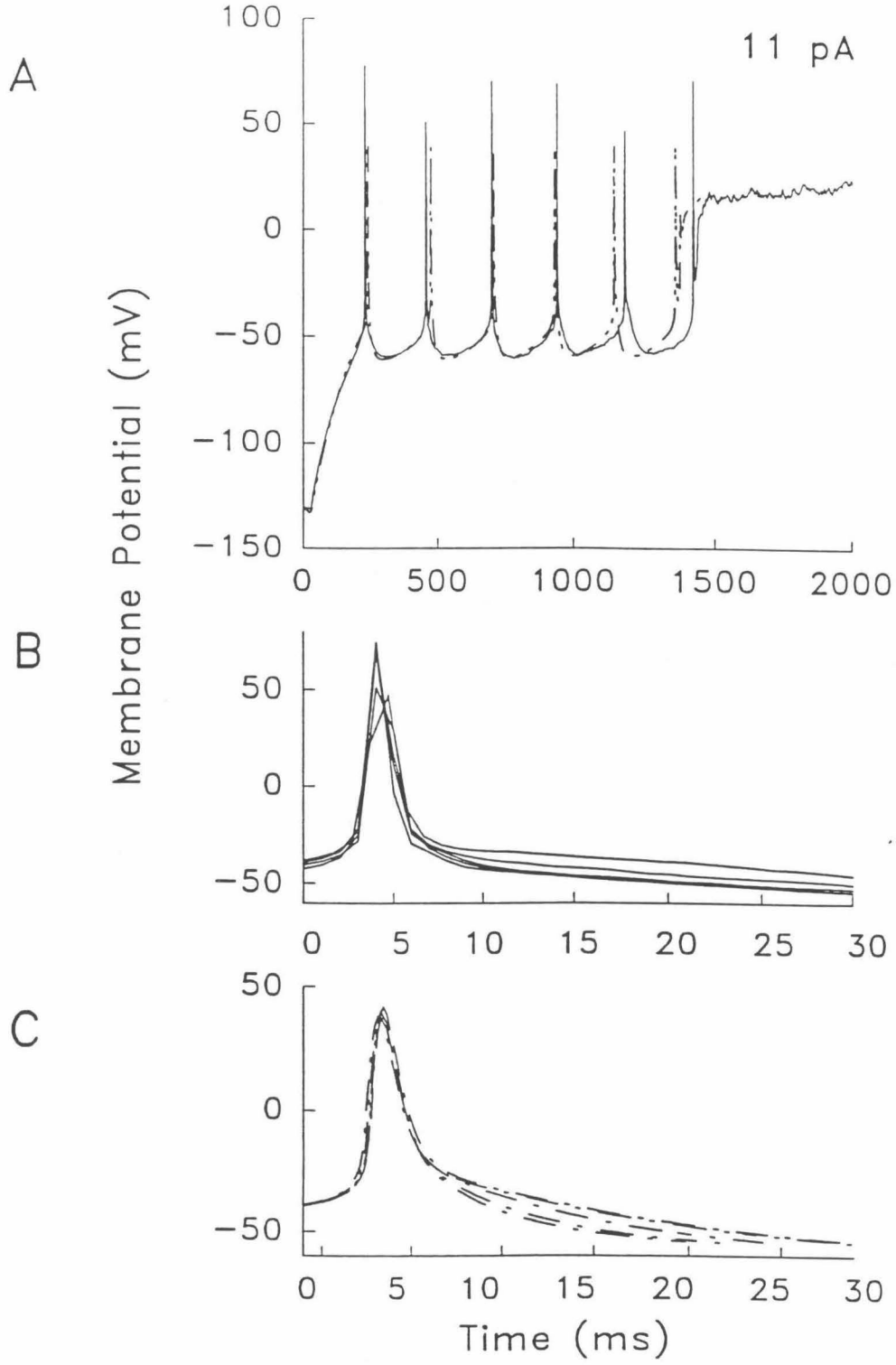

Figure 12. Lock-up of Membrane Potential at Larger Stimulus Current.

Figure 12. Lock-up of Membrane Potential at Larger Stimulus Current.

(A) Recorded (solid traces) and simulated (dashed traces) voltage trajectories from the exemplar cell during the same series as Fig. 6. (B) Superposition of all the action potential waveforms from (A). Note the progressive elevation of interspike trajectories. (C) Superposition of the simulated action potentials, again showing the progressive elevation of interspike trajectories depending on the initial firing frequencies.

"C-type" inactivation (Hoshi et al, 1991). That interspike intervals did not vary until "lock-up", despite the gradually decreasing K channel availability that gradually eliminated the hyperpolarizing after-potential, suggests that the K^+ currents did not strongly affect the interspike interval. Although the hyperpolarized resting potentials in cells expressing only K^+ channels suggest that a small fraction of these channels never inactivate, this fraction was evidently too small to prevent the depolarized plateau; we estimate that it was less than ~0.1% of the peak K^+ conductance.

Fluctuations in Membrane Potential and Spontaneous Firing

Examples of the membrane potential fluctuations are illustrated in Figure 13. Such fluctuations occurred despite a constant holding current and could be observed in all cells when examined at higher resolution. The magnitude and frequency of these fluctuations increased with the membrane potential. The control, mock-transfected cells also exhibited similar fluctuations in membrane potential, although the amplitude of the fluctuations was smaller than in cells expressing Na^+ and K^+ currents and were not dependent on the membrane potential. The nature of these fluctuations is unclear. Nevertheless we postulate that they are caused by random opening and closing of ion channels. We also observed spontaneous action potentials in the absence of any holding or stimulus currents. They probably resulted from the membrane potential fluctuations. In order to see the spontaneous activity it was necessary to first hyperpolarize the cell to less than -100 mV to remove Na^+ channel inactivation which occurred at the -40 mV to -55 mV resting potentials. Then the cells fired spontaneously at irregular intervals that lasted up to 15 min.

Under prolonged stimulation, up to several minutes, repetitive firing could not be maintained for more than 5 s. Instead, the electrical activity of the artificial neuron tended to fall into two categories. At high frequencies, the cell fired regularly for a few seconds and then the membrane potential locked up (Figure 14) for reasons outlined above. Following low to intermediate initial firing frequencies for also just a few seconds, action potentials first stopped and then continued to occur, but mostly at irregular intervals (Figure 15). We propose that this irregular firing under constant stimulation also results from the membrane potential fluctuations.

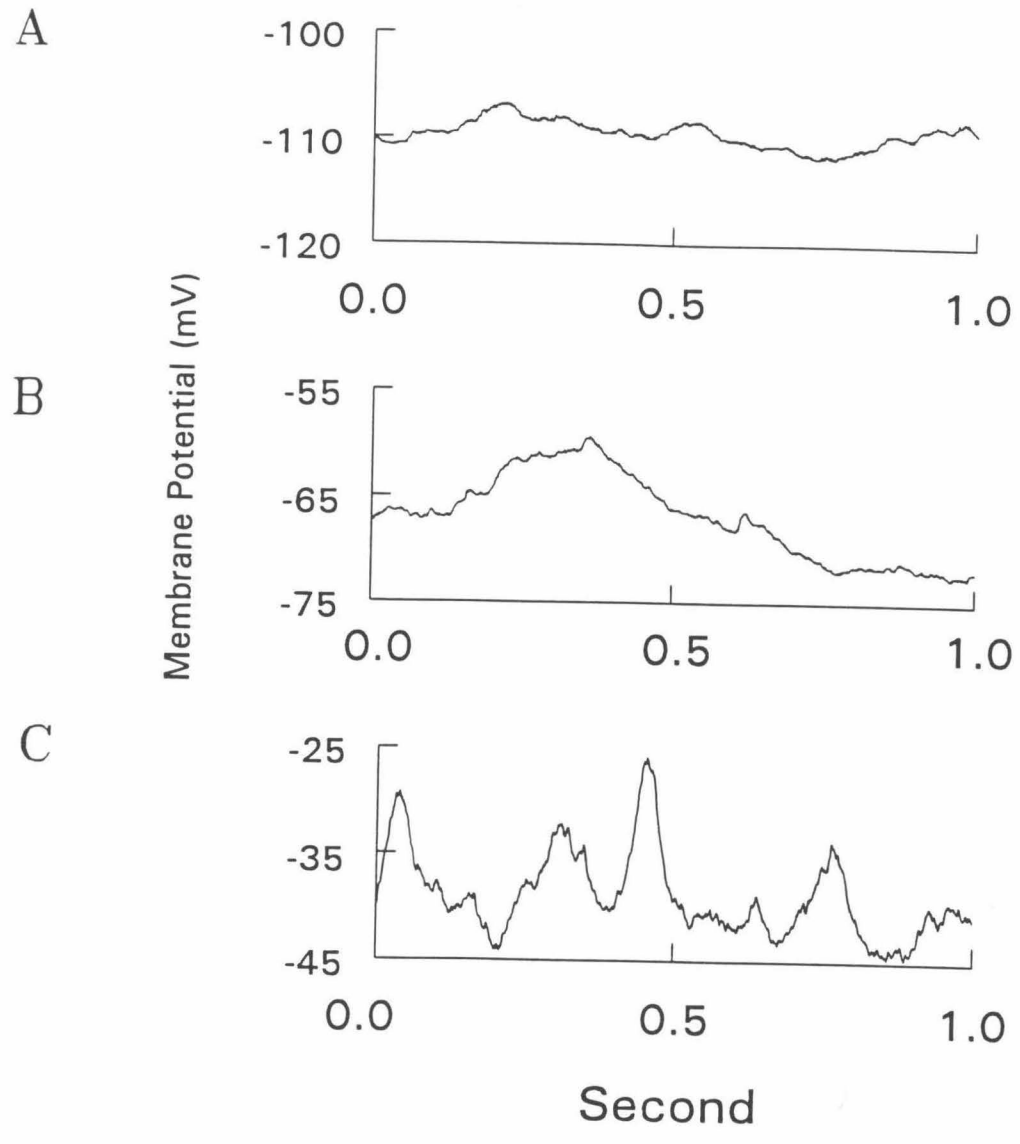

Figure 13. Membrane Potential Fluctuations. Examples of membrane potential fluctuations in (A), (B) and (C) are from the same cell. The holding currents are -100 pA (A), -40 pA (B) and -20 pA (C). Both magnitude and frequency of these spontaneous potential fluctuations are voltage dependent. The sampling rate for all traces is 2 kHz.

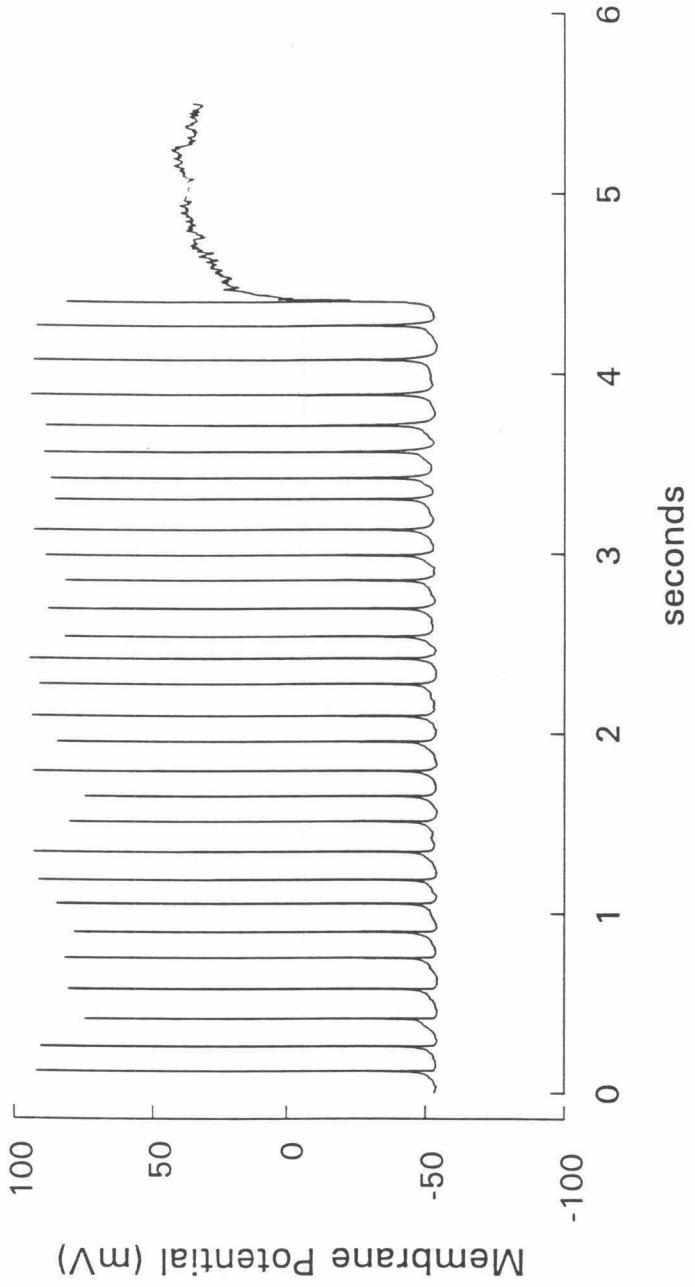

Figure 14. Lock-up of Membrane Potentials under Prolonged Stimulation.

The holding current is -40 pA and the stimulus current is 10 pA for 5.5s. The sampling rate is 2 kHz.

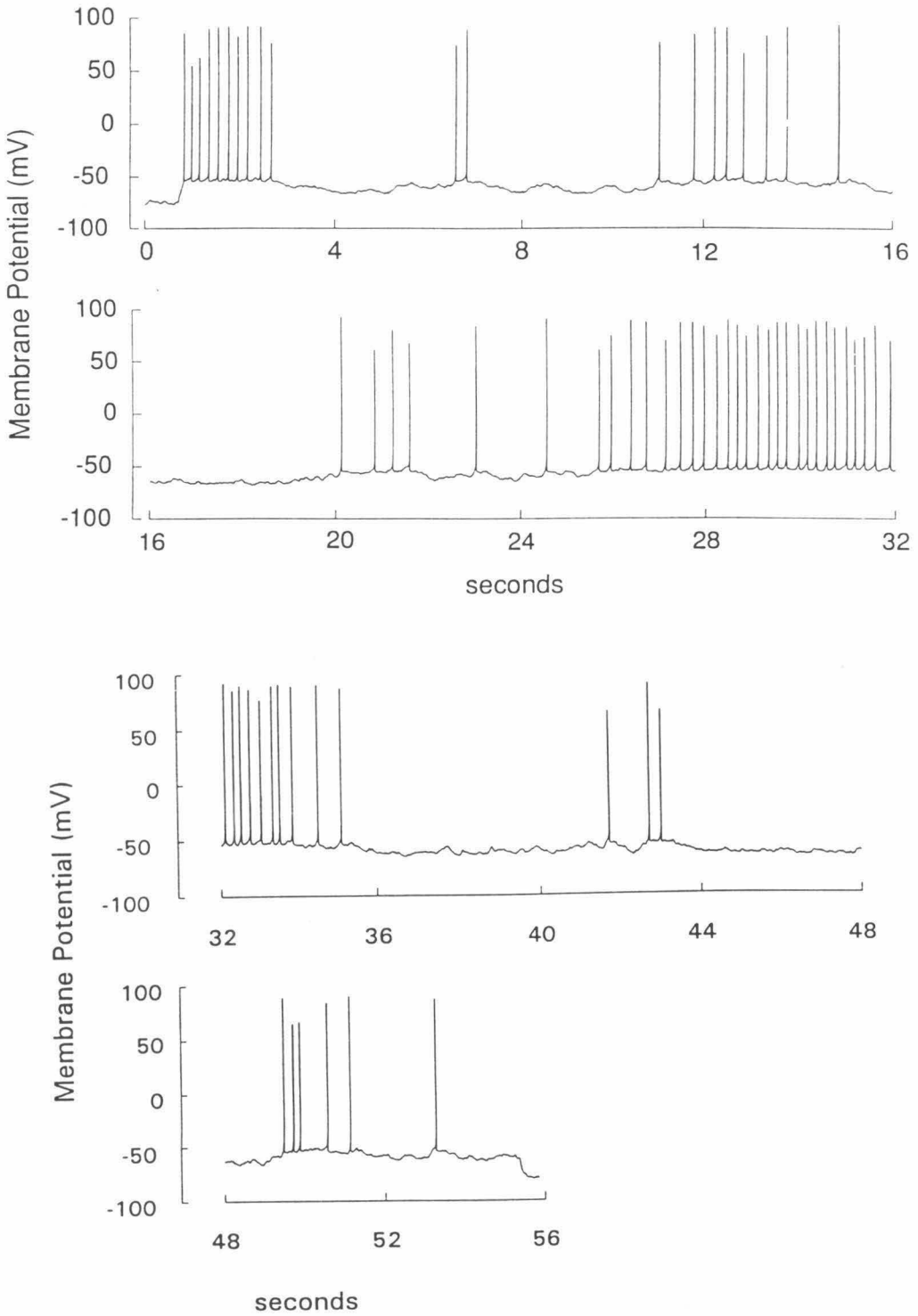

Figure 15. Irregular spike activity under prolonged stimulation.

Figure 15. Irregular spike activity under prolonged stimulation.

The holding current was -40 pA and the stimulus current was 8 pA for 55 s. Action potentials fired at regular intervals for the first 3s and then stopped. Irregular spike activity resumed for the duration of the stimulus. The sampling rate of 2 kHz was not fast enough to record all of the action potential peak. Hence the data show variations in action potential peak amplitudes.

Graded action potentials

Graded action potentials, in contrast to the familiar all or none action potentials have a shape and amplitude that depends on the strength of the stimulation. This type of action potential occurs in neuronal development, and cultured hippocampal neurons (Johansson et al, 1992a). Graded action potentials are also observed in the artificial neuron system (Figure 16). Preliminary analysis of this phenomenon showed that the peak K current must be at least 4 times higher than the peak Na^+ current (5 cells) in order for this activity to be observed. Moreover simulations showed that there exist a critical Na^+ channel density above which all or none action potential occurred, and below which graded action potentials occurred. Potassium channel density influenced the width of the graded action potentials.

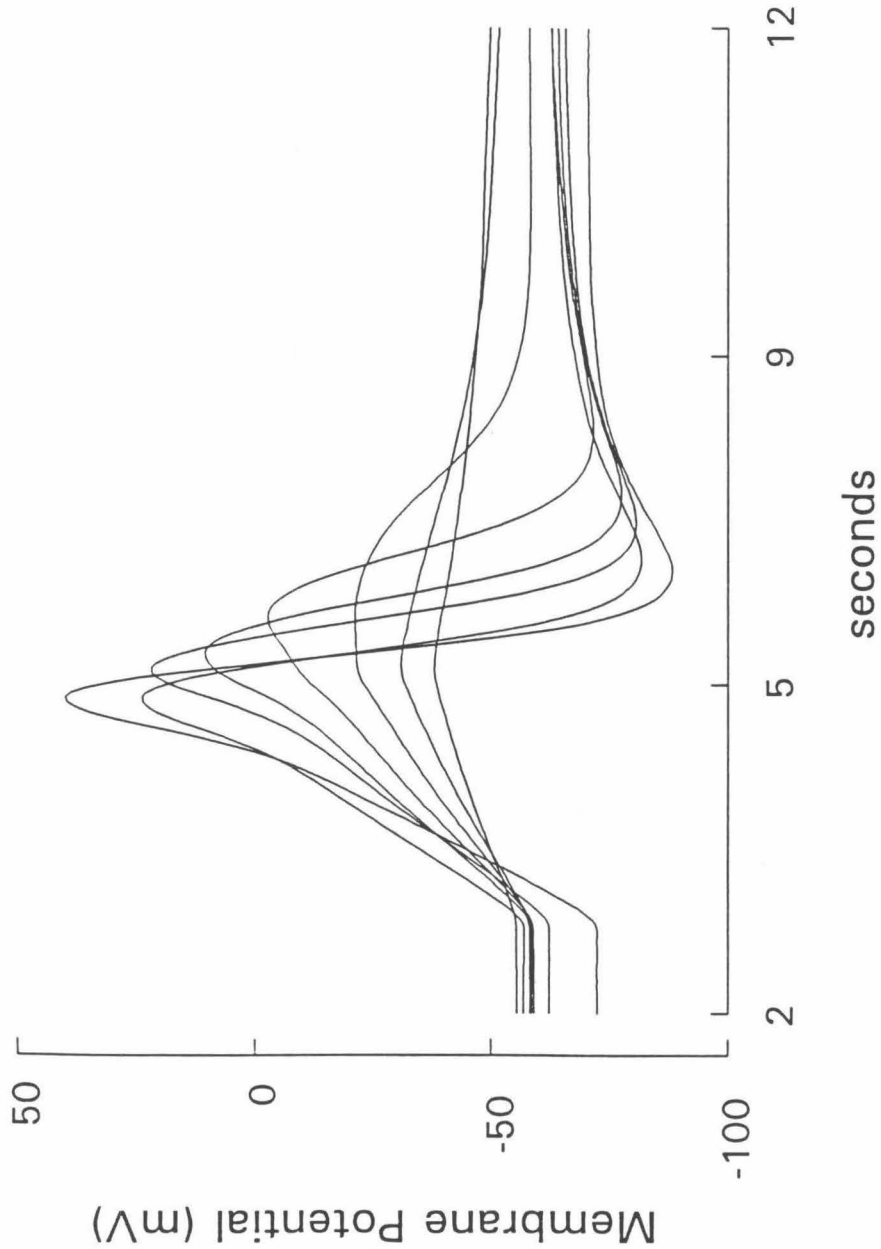

Figure 16. Graded Action Potential.

In traces 1-7, the holding current was -120 pA and the stimulus current ranged from 100 pA to 400 pA in increment of 50 pA. In trace 8, the holding current was -80 pA and the stimulus current was 480 pA.

Chapter Four
Numerical Model of the Artificial Neuron

Description of the Numerical Model

To test our understanding of the encoding properties of the synthetic neuron, a numerical model for an exemplar cell was constructed. The schematic diagram of the numerical model is shown in Figure 17.

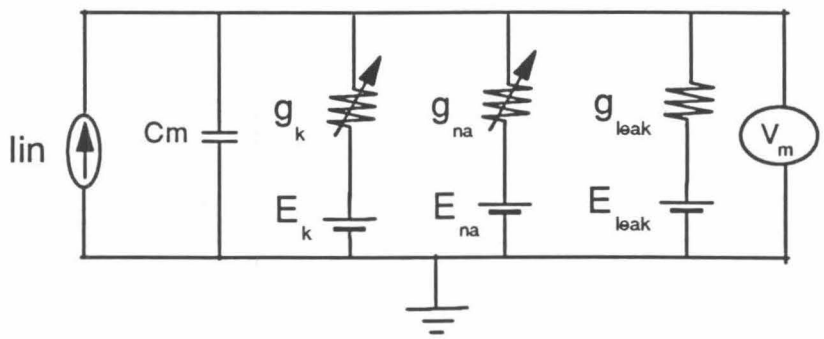

Figure 17. Schematic Diagram of the Numerical Model.

The cell membrane is modeled as a capacitance (C_m) in parallel with a resistance (g_{leak}) powered by a battery E_{leak}. The Na^+ and K^+ channels are modeled as variable resistors g_{na} and g_k powered by batteries E_{na} and E_k, respectively.

The parameters for steady-state activation and inactivation (m_∞ and h_∞) were obtained from Yang et al (1990) for Na^+ channels and from Hoshi et al (1990) for K^+ channels. To confirm that the behavior of these channels did not change in our experiments, we analyzed steady-state properties of Na^+ and K^+ channels in the artificial neuron for at least 5 cells. Time constants of fast activation and inactivation (τ_{m1} and τ_{h1}) for both Na^+ and K^+ channels were determined from fitting the rising and falling phases of the voltage-clamped currents and are similar to published results (Yang et al, 1992; Hoshi et al, 1991; Leonard et al, 1989; Stuhmer et al; 1989; Catterall et al , 1991). The time constants of slow inactivation (τ_{h2}) were measured according to protocols illustrated in Figures 7 and 9. However, all time constants from -100 mV to -40 mV were estimated by simulating the voltage trajectories. Kinetic measurements were impossible because ionic currents were not activated at these voltages. E_{na} and E_k were determined from tail current analysis and were also similar to published results (Hoshi et al, 1991; Iverson et al, 1990). For the exemplar cell, channel density (g_{max}) was calculated from measurements of maximum currents and cell capacitance.

Simulations were performed on UNIX workstations running the NEURON program (Hines, 1989) for a single-compartment cell. The following equations, based on Hodgkin and Huxley (1952), were integrated numerically, where I is membrane current, C_M is membrane capacitance, V is potential, and E_i is the Nernst potential for conductance i (Na^+, K^+ , or leak):

$$I = C_M \frac{dV}{dT} + \sum I_i;$$

$$I_i = \overline{g}_i (V - E_i) m_i^3 [\varepsilon_i + h_{1i}(1 - \varepsilon_i)] h_{2i};$$

$$\frac{dm_i}{dt} = \frac{m_{\infty i} - m_i}{\tau_{mi}};$$

$$\frac{dh_i}{dt} = \frac{h_{\infty i} - h_i}{\tau_i};$$

For each τ, we define

$\tau = 1/(\alpha + \beta)$.

For the leakage conductance, we define

$m_{leak} = h_{leak} = 1; \qquad E_{leak} = -10$ mV.

We simulated the voltage trajectories for 5 cells that yielded our most complete data. Figures 11, 12, 14, 19, and 20 present recorded and simulated data from a single exemplar cell; only minor changes in the parameters accounted for the other four cells studied in detail. The formal model for the K^+ conductance was identical to that for the Na^+ currents, with two inactivation parameters *h1* (fast) and *h2* (slow). The values for these parameters were based on experiments during this series and on previous (Leonard et al, 1989) studies. To the equations for Na^+ activation and inactivation, given above (Chapter 3, p23), we added equations for K^+ activation,

$$m_{\infty,K} = \frac{1}{1 + \exp\left(-\frac{V + 27}{10}\right)};$$

$$\alpha = \left[\frac{320}{1 + \exp\left(\frac{V + 49}{2}\right)} + 3.6 \exp\left(-\frac{V}{25}\right)\right]^{-1};$$

$$\beta = 3.6\left[1 + \exp\left(\frac{V + 66}{-10}\right)\right];$$

and for K^+ inactivation,

$$\varepsilon_K = 0.11;$$

$$h_{1\infty,K} = h_{2\infty,K} = \frac{1}{1 + \exp\left(\frac{V + 29}{3.5}\right)};$$

$$\alpha_1 = 0.018 \exp\left(-\frac{V + 70}{17}\right);$$

$$\beta_1 = \left[\frac{385}{1 + \exp\left(\frac{V + 34}{4}\right)} + 4\right]^{-1};$$

$$\alpha_2 = 3.75 \times 10^{-5} \exp\left(-\frac{V + 40}{15}\right);$$

$$\beta_2 = 0.0025 \exp\left(\frac{V}{19}\right);$$

In this formalism, the case $\varepsilon_K = 0$ would correspond to a K^+ current that inactivates on a time course of ms (governed by the kinetics of h_1; while $\varepsilon_K = 1$ corresponds to a much slower inactivation, with a time constant of 400 ms at zero mV in this case. Intermediate values for ε_K represent a current that declines rapidly to a fractional value of ε_K, then slowly to a smaller value.

Firing Frequencies

In this formalism, we are able to simulate the voltage trajectories of the exemplar cell (Figures 11, and 12). The following points emerge from the simulations. (1) The simulations reproduced the wide range of firing rates and the relation between firing rate and applied current. Between spikes, K^+ conductance remains activated. At 7 Hz K^+ current can be as much as +15 pA (outward) while the algebraic sum of all currents is less than 1 pA and inward. Deactivation and inactivation of K^+ conductance from -40 mV to -60 mV plays a dominant role in determining the firing rate. (2) On the other hand, at frequencies below 2 Hz, the membrane potential is repolarized to E_K and the remaining K^+ current is negligible (less than 0.5 pA). The precise kinetics of K^+ conductance no longer influence the firing rate. The important parameters are the passive resistance and capacitance of the cell. (3) The slow inactivation of K^+ conductance accounts for the lock-up phenomenon at firing rates below 5 Hz. With each impulse, h_2 decrements 3-5%, leading to a cumulative inactivation over several impulses (Figure 20A). When insufficient K^+ conductance remains to repolarize the cell, the membrane potential attains a value determined by the injected depolarization current and by the residual non-inactivated Na^+ conductance. Finally, when the interspike interval is long enough to allow even slow inactivation to recover, the cell in theory will fire indefinitely. (4) At firing rates above 5 Hz, fast inactivation of K^+ conductance (controlled by h_1), accounts for the lock-up (Figure 20B). With each action potential, h_1 decrements by 50-55%, then recovers with time constants from 80 ms at -30 mV (as recorded by Leonard et al, 1989) to a peak value of 120 ms at -60 mV. This long

recovery time limits the maximum frequency to 15 Hz in most cells. (5) Repetitive firing frequencies did not depend strongly on the detailed kinetics of Na^+ activation and inactivation ($\tau_{m,Na}$, $\tau_{h1,Na}$, $\tau_{h2,Na}$) but did require the noninactivating "window currents" that occur between -30 mV and -50 mV at the overlap between steady-state activation and inactivation $\left(m_{\infty,Na},\ h_{1\infty,Na},\ h_{2\infty,Na}\right)$. In particular, the simulations reproduced the experimental finding that lock-up occurs more quickly as the firing frequency increases (Figure 18).

In the simulations, *f/I* (Figure 18A), the slope of frequency (*f*) vs. stimulus current (*I*), depends only weakly on Na^+ or K^+ current but shows a roughly inverse dependence on cell size; this agrees with the experimental finding that the slope decreased with larger capacitance (Figure 22). The basis for this phenomenon is that at low firing frequencies, the interspike interval is determined by charging of the cell capacitance. In the simulations, cells with K^+ channel density lower than ~ 1 nA/pF locked up at lower firing frequencies than did cells with densities greater than 1 nA/pF, as found experimentally.

There remains one untested point in our numerical simulations. We found it necessary to employ rate constants for Na^+ activation/deactivation, $\tau_{m,Na}$, that increased significantly at potentials more negative than -50 mV. This formulation suggests that Na^+ "tail currents" should be relatively long (up to 20 ms) at such potentials. This prediction deserves systematic study.

There also remain a few discrepancies in our numerical simulations. (1) The voltage trajectories are best simulated with a Na^+ current density for each cell twice that recorded in the voltage-clamp experiments. We believe that this discrepancy arises from artifactually low Na^+ current measurements, due to inadequate voltage-

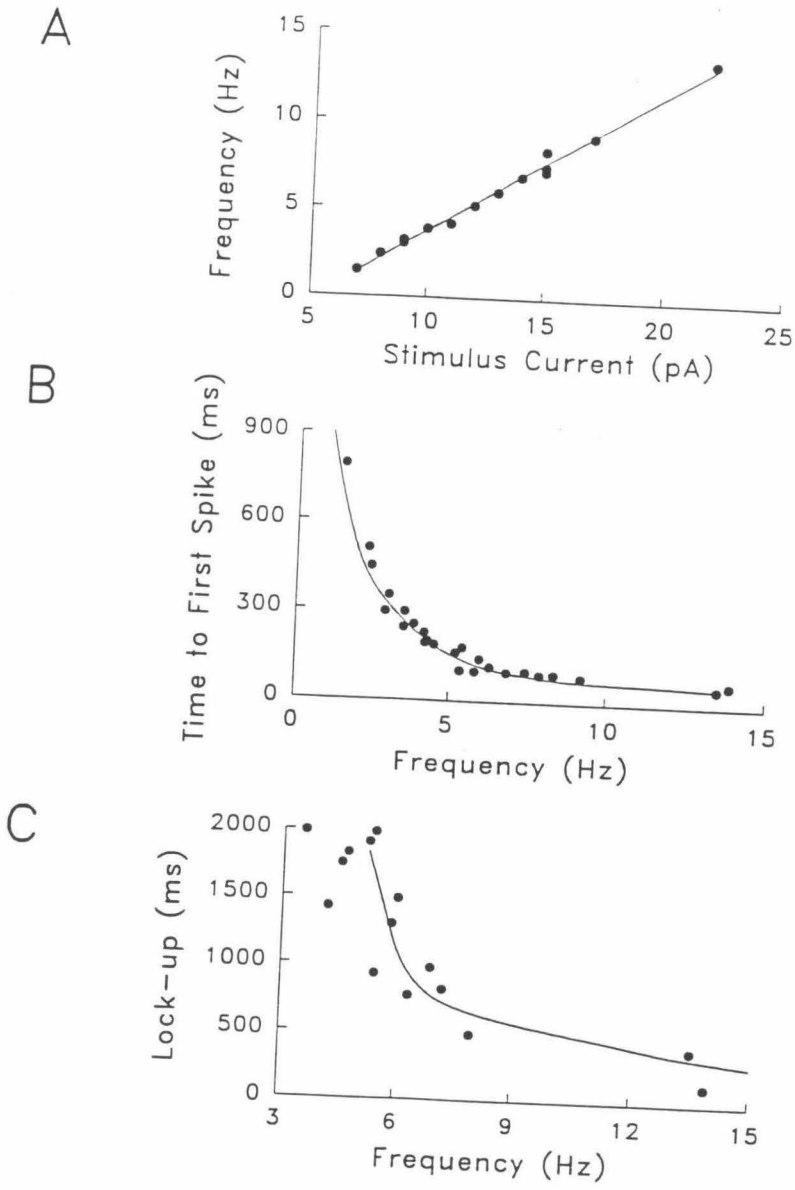

Figure 18. Analysis of the Voltage Trajectories of the Exemplar Cell.

(A) Firing frequency as a function of stimulus amplitude for recorded data (symbols) and simulated data (lines). (B) Time to first impulse as a function of firing frequency for recorded data (symbols) and simulated data (line). (C) Analysis of lockup. Ordinate, time to lockup. Abscissa, firing frequency. Symbols, recorded data; solid line, simulated data.

clamp fidelity. (2) The simulated peaks are also 20-30 mV less positive than the recorded peaks; this discrepancy probably arises from under-damping in the patch-clamp headstage used in the current-clamp mode (R. Lobdill, personal communication).

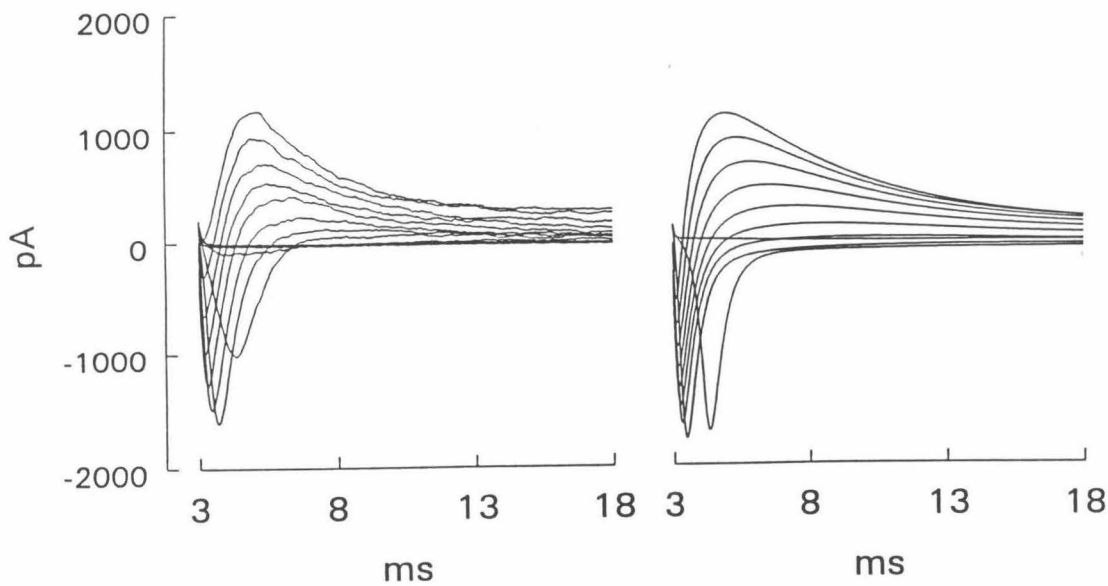

Figure 19. Recorded and Simulated Ionic Currents of the Exemplar Cell.

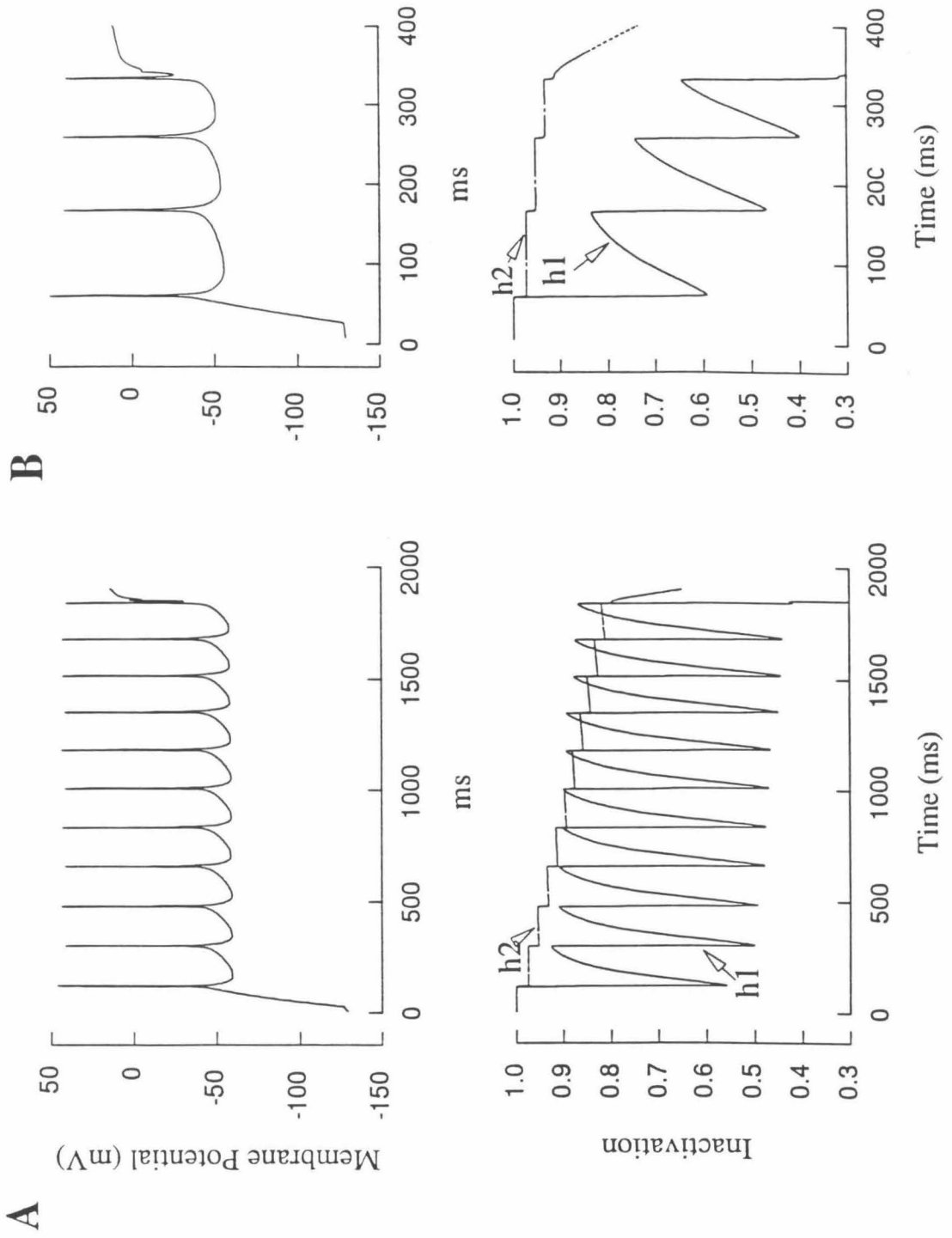

Figure 20. Analysis of K^+ Current Inactivation During Voltage Trajectories Leading to Lock-up.

Figure 20. Analysis of K^+ inactivation during voltage trajectories leading to lock-up.

(A) At firing rate below 7 Hz, h_1 decrements by 50-55 % with each impulse but recovers almost completely during the interspike interval. However, h_2 decrements 3-5% during each spike, leading to a cumulative inactivation over several impulses. When insufficient K^+ conductance remains to repolarize the cell, the membrane potential locks up. (B) At firing rates above 7 Hz, changes in h_1 dominate the lock-up. With each action potential, h_1 still decrements by 50-55%; but there is insufficient time for complete recovery during the interspike interval. Notice the two different time scales of (A) and (B).

Delayed Excitation

We examined the role of K^+ currents in the delay in excitation, that is, the time between the application of a stimulus current and the firing of an action potential. In real neurons, when this delay is many times longer than the time constant of the cell, turning on of potassium currents who are activated at subthreshold voltages during this delay is often implicated (Connor and Stevens, 1971a, b and c; Storm 1988). In our simulations, potassium currents are not activated at subthreshold voltages. Surprisingly, the asymptotic charging of membrane capacitance accounted for most of the long delay in excitation; addition of K^+ currents in the simulations prolonged the delay by a mere 20% (Figure 21A). In both experiments and simulations the delay showed strong dependence on the resting potential, firing frequency and stimulus current in agreement with data obtained from nervous systems (Storm, 1988). In light of the findings for K currents, the mechanisms that underlie delayed excitation in the nervous system require further examination.

Minimum Frequency

We wanted to determine what acting ionic current might be responsible for prolonging the interspike interval and maintaining the 1-2 Hz low spike frequencies. However, the simulation data showed almost no active currents. The membrane potential during the interspike interval at low frequencies was charged to threshold by the stimulus current only. Two results support this conclusion. First, simulations showed that the magnitude of K^+ current during interspike intervals was a mere one-hundredth of the stimulus current at 1 Hz and only one-tenth of the stimulus current at

2 Hz. The charging of membrane potential during interspike interval is linear with respect to time. On the other hand at 5 Hz, the magnitude of interspike K^+ current increases to 80% of the stimulus current and the charging of the membrane potential is non-linear. Second, experimental observations show that the delay to the first action potential at 1-2 Hz firing frequencies is almost the same as the interspike interval at these frequencies (Figure 21B). This suggests that charging of the membrane potential during low frequency interspike intervals has the same mechanism as the delay in excitation (Figure 21A).

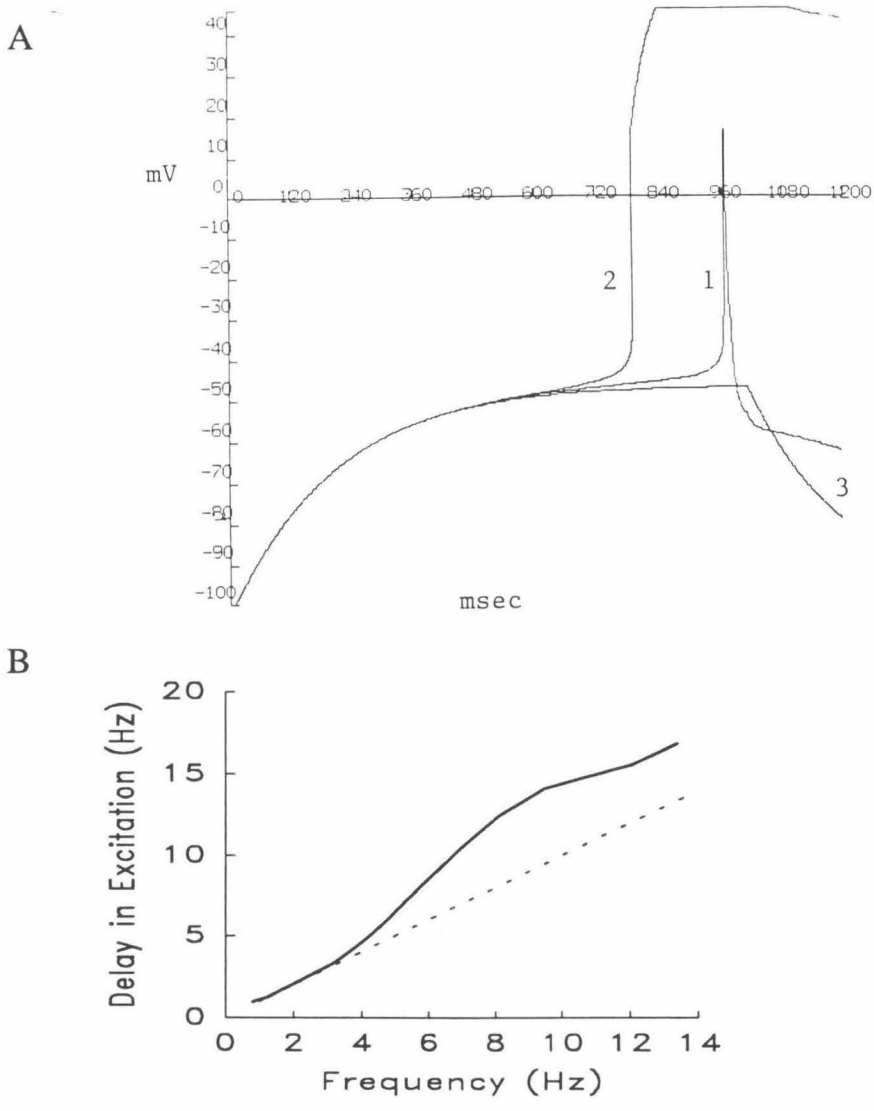

Figure 21. Simulation of the Delay in Excitation.

(A) The charging of membrane potential to threshold when both Na^+ and K^+ channels are included in this simulation (trace 1), only Na^+ channels are included (trace 2) and no channels are included (trace 3). The addition of K^+ channels delays the generation of an action potential by 20% longer than with Na^+ channel alone. (B) A replot of Figure 18B. The solid line is the simulated data and the dotted line has slope equal to one.

Current-Frequency Relationship

Although K^+ current directly influenced spike frequencies, the largest effects on the slope of the *f/I* curve was correlated to the changes in cell capacitance (Figure 22). This means that for small cells, firing frequencies are more steeply dependent on the stimulus current than for large cells. It does not seem plausible that the nervous system would modulate its information processing ability by changes in cell size; but during development, varing cell size would be an energy efficient way to hardwire the central nervous system with divergent encoding properties.

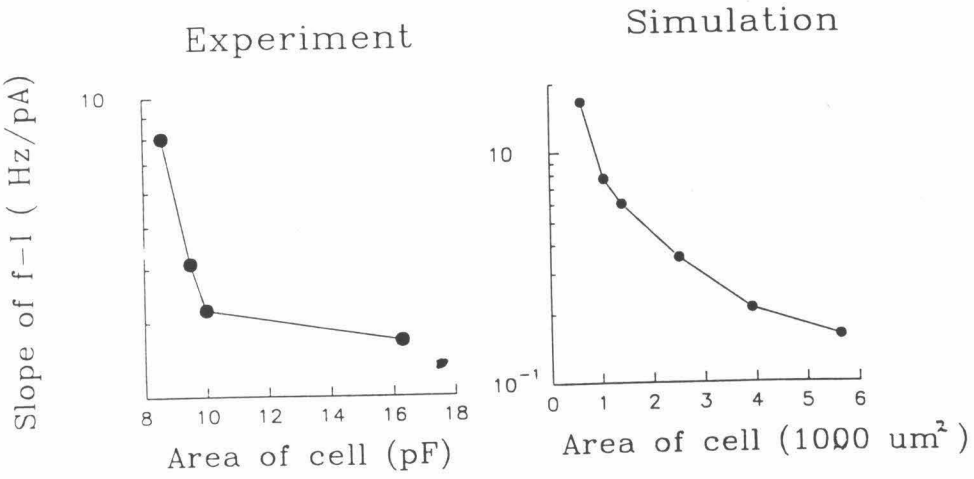

Figure 22. Dependence of Firing Rate on Cell Membrane Capacitance. Recorded (A) and simulated (B) data of the slope of frequency versus stimulus current plotted against the cell size. The slope of the frequency-current *f/I* relationship is plotted on a log scale to illustrate the sharp drop in *f/I* slope as cell size increases.

Chapter Five
Discussion

The synthetic neurons display moderately complex encoding properties. When cells express only Na^+ channels, the action potentials have long plateaus that resemble cardiac action potentials (Figure 6). With only 2 channel types--a Na^+ and a K^+ channel--the experiments provide the unusual opportunity to study encoding properties of cells lacking the classical "delayed rectifier" found in nearly all excitable cells. Even so, the trajectories include such interesting features as a wide dynamic range of firing frequencies (Figure 19A), time-dependent changes of the action-potential waveform (Figure 12B), and "lockup" after several seconds of stimulation (Figures 12A, and 14). The broad dynamic range of firing frequencies resembles that of many real neurons. Some of these properties might have been predicted on the basis of the original voltage-clamp records from the cloned and expressed Na^+ IIA and Shaker H4 channels. Our study emphasizes that interactive experiments and simulations on synthetic neurons provide a decisive strategy to account for focusing on the important properties of the individual excitable channel populations that account for the voltage trajectories in a cell.

In general, we acknowledge that our equations and parameters, based on the Hodgkin-Huxley (1952) formalism, may represent only one of several possible formal descriptions that would adequately simulate the voltage trajectories. However, we devoted considerable effort to simulations that omitted slowly inactivating Na^+ and K^+ conductances; other such models could not account for the plateau and "lock-up". We therefore have confidence in the conclusion that slow channel kinetics do underlie

these slow components of the voltage trajectories. Furthermore, the non-inactivating Na^+ "window currents" were essential for explaining the long interspike intervals we observed.

Role of Transient K^+ Currents in Repetitive Firing

It has long been thought that transient K^+ channels ("A" channels) play an important role in determining repetitive firing activity of neurons by broadening the range of input currents over which repetitive firing occurs (Connor and Stevens, 1971a, b, and c). Our study confirms this concept but adds new insights. In particular, (1) such channels help to determine the interspike interval for moderate depolarizations and spike rates. Shaker H4 channels activate at a considerably more positive voltage than do most A channels in neurons (Rudy, 1988); nonetheless, once they are activated by an action potential, they appear to deactivate so slowly that they do contribute to the next interspike interval. It would be instructive to repeat the present experiments with a transient K^+ channel that activates at more negative potentials. (2) It is often thought that, for large depolarizations, the K^+ channels inactivate and no longer control the voltage trajectory during the interspike interval and that this effect helps to produce a large dynamic range of firing frequencies (Connor and Stevens, 1971a, b, and c). This point can be tested with high sensitivity in the present simple synthetic neurons, for there is no other K^+ conductance to limit the depolarization during the interspike interval. In most of our cells, the firing frequencies for larger input currents remain constant during a given train as the transient K^+ channels inactivate, even until just before lockup (e.g., Figures 12 and 14). However, simulations of Figure 20B do suggest that a shortened final interspike interval might be observable with the largest depolarizing currents.

Relevance of Synthetic Neurons

The data and simulations suggest that slow inactivation (termed C-type inactivation by Hoshi et al, 1991) of transient K^+ currents is not an epiphenomenon but could play a role in encoding properties of real neurons. For a typical sustained depolarization, many times more current would flow through these channels during the long , slow phase than during the larger but much briefer early peak. On the other hand, inactivation of transient K^+ currents has previously been invoked to explain spike broadening by depolarization (Belluzzi et al, 1985). Such broadening may have functional consequences because it increases the amount of transmitter released from presynaptic terminals (Klein et al, 1982; Augustine, 1990; Kaang et, 1992).

C-type inactivation also occurs for K^+ channels, such as Kv3, that are maintained for several tens of ms (Marom et al, 1992). In the case of Kv3, C-type inactivation can be modulated (Marom et al, 1992), raising the possibility that external influences could control the effects of such inactivation on voltage trajectories.

The Role of High Impedance

Action potential waveforms with prolonged plateaus are typical of cardiac cells, for instance Purkinje fibers and ventricular myocytes, and are rarely observed in neurons. However, in previous experiments where (a) only Na^+ channels were stimulated, (b) voltage-dependent K^+ channels were eliminated, and (c) resting conductances were very low, similar plateaus have been observed (Chandler and Meves, 1970d). The CHO cells used in the present studies present a similar situation.

With few or no endogenous channels, their membrane potentials are sensitive to even the small component of slowly inactivating Na^+ current in our experiments. Our simulations show how the plateau results from this set of factors. While this low background conductance contributes to the interesting encoding mechanisms we have observed, is it relevant to real excitable cells? The literature suggests that it is. As a first example, Hille (1991, pp. 128-129 and 193-197) argues that the low density of background conductance (1) allows cardiac muscle to spend a percentage of time depolarized with only a moderate metabolic load and (2) allows modulation of small currents to influence encoding properties. It has often been asked whether the plateau phase of the cardiac action potential is governed by incomplete Na^+ channel inactivation as well as by the slow Ca^{2+} conductance. Some experiments in the literature suggest that this is the case, because TTX shortens the plateau phase (Grant and Starmer, 1987). The experiment of Figure 6 is a decisive demonstration of this point, because we know that Na^+ channels are the only ones open during the plateau. As a second example of the relevance of low background conductance, recent patch-clamp recordings in brain slices reveal much lower background conductance than previously suspected (Blanton et al, 1989; Edwards et al, 1989; Andersen et al, 1990). Thus our experiments may provide a model for neurons as well as cardiac cells.

Between impulses, a neuron's membrane potential is typically between -40 mV and -60 mV. The synthetic neuron demonstrates that kinetics of channel conductance at these potentials directly determine the firing rate. A small change in these kinetics can dramatically alter dynamic properties. All channels have "window currents" that do not inactivate. In cells with low impedance, these sustained currents are negligible compared to the background current. In the synthetic neurons, the high impedance unmasks these small, slow changing currents. They contribute significantly to the

shape of the interspike waveform and the firing rate. The high impedance enables the cell to integrate currents just a few pA in amplitude.

Resting Membrane Potential

In the artificial neuron, potassium "window" current alone could account for the hyperpolarized resting potentials. This window current in theory should be sensitive to pharmacological blockers. CHO cells with their high input resistance are an ideal preparation to study the quantitative relationship between resting potential and potassium window current. A systematic study of this relationship may help us understand the ionic components important for determining the background conductance of real neurons.

Mammalian Potassium Channels

Slow inactivation of K^+ channel was also confirmed in current clamp experiments. In all 8 repetitive firing cells, the first few current stimulation did not yield repetitive spikes. Membrane potentials often exhibited depolarizing afterpotentials. Thus we found it necessary to hyperpolarize the membrane to -120 mV for 2-5 minutes to remove K^+ channel slow inactivation in order to produce repetitive spikes. Shaker-like potassium channel genes have been mapped throughout the mammalian nervous system (Sheng et al, 1992; Stuhmer et al, 1989; Tseng-Crank et al, 1990; Roberds and Tamkun, 1991). Comparing the properties of mammalian and *Drosophila* transient potassium channels shows that the rat cardiac gene and Shaker H4 have almost identical properties (Tseng-Crank et al, 1990). The major

difference between the rat brain transient K^+ channel and the Shaker H4 channel is in their activation and inactivation voltage ranges. The brain channel is activated and inactivated in a range 30 mV more negative than H4 (Stuhmer, 1989). This type of transient potassium current has been shown to directly control firing frequencies (Connor and Stevens, 1971a, b, c) and hence the slope of *f/I* curve. Our simulations show that a negative shift in voltage-dependence of either the K^+ channel activation or inactivation curves does not significantly alter the firing properties of the artificial neuron. Analysis of the simulations show that subthreshold activated K^+ channels even though open at these subthreshold voltages, conduct little current because the driving force is small. Instead we find that the kinetics of K^+ channel between -40 to -55 mV have a more profound effect on the electrical activity.

The rapid cloning of K^+ channel genes reveal that their channels belong to a very large and diverse gene family. Not surprisingly, expression of the K^+ channels reveals that this family displays a wide range of biophysical and pharmacological properties. The distribution of these genes in the brain show selective and regional localization (Rettig et al, 1992; Surmeier et al, 1989). Addition of these genes in the artificial neuron, one or a few at a time, should help identify the specific biophysical characteristics important for determining the encoding properties of real neurons, as we have shown here for the NaIIA and Shaker H4 channel genes.

Spontaneous Spikes

Spontaneous spikes (Johansson, 1992) have been observed in cultured hippocampal neurons and hippocampal granule cell layer. They are attributed to the

spontaneous synaptic events (Dudek et al, 1976; MacVicar and Dudek, 1982; Fournier and Crepel, 1984). Spontaneous spikes are also present in the artificial neuron. Since the artificial neuron has no synaptic contact with any other neurons, this spontaneous activity must be caused by the spontaneous opening and closing of ion channels. Analysis of this possibility in the artificial neuron suggests that small neurons with high membrane resistance in the central nervous system could fire spontaneously at low and irregular intervals. Such background firing activity could be important to the function of the whole network by priming circuits when no external stimuli are present.

Limitations and Possibilities of the Synthetic Neuron System

Real neurons have many more channel types than the synthetic neurons reported here (Llinas, 1988). The obvious conductance type lacking in our present synthetic neurons is a maintained K^+ conductance ("delayed rectifier") which would eliminate the "lock-up" (Fig. 5B) by providing a K^+ conductance with $\tau_h = \infty$. Experiments in progress are aimed at introducing such a conductance. With regard to the possibility of modulating the firing rates via intracellular messengers, the vaccinia system has also been used to introduce serotonin $5HT_{1A}$ receptors into mammalian cardiac cells, where they couple via endogenous G proteins to a class of endogenous K^+ channels important in regulating impulse frequency (Karschin et al, 1991b). Thus it also seems possible to employ vaccinia or other mammalian cell expression systems to investigate the control of encoding properties by neurotransmitters in cells that are already endowed with a set of endogenous channels, receptors, or transporters.

In addition to the larger repertoire of channels, receptors, and transporters in real neurons, these molecules may be localized differentially in several physically and electrically isolated regions of the cell. Although correct targeting and sorting has been reported for vaccinia virus expression in epithelial cells (Stephens et al, 1986), it is not known whether such processes will occur in neurons with the vaccinia expression system.

The major limitation of the vaccinia expression system is the wide variability of expression levels among cells in the population. Only 20% of the cells in our experiments expressed Na^+ and K^+ channels in the range of ratios that gave repetitive firing. The percentage of satisfactory expression would presumably decrease even further if three or more channel types were employed. We suspect that the most appropriate system will be one in which (*1*) a cell line is constructed that stably expresses a basic set of channels--for instance, the two studied here--and (*2*) additional channels are added using the flexible and rapid vaccinia system.

Future Improvements on the Expression Efficiencies

A promising prospect for improving the overall success rate of recording cells expressing both Na^+ and K^+ channels is co-transfection of a marker gene for which there is a non-lethal chromogenic or fluorescent substrate. Thus, cells likely to be expressing ion channels could be identified through visible or fluorescence microscopy. Only the marker-positive cells would be assayed electrophysiologically. At present four different genes have been successfully expressed simultaneously and with high

efficiency using a fluorescent substrate and marker gene combination protocol (Angelotti et al, 1993).

Future Directions

Most importantly, addition of a sustained potassium current to the artificial neuron is essential for the stability of the electrical activity. The unique advantages of the artificial neuron preparation can also be used to study the interesting and currently fashionable topics of neuronal modulation by protein kinases. For example, the artificial neuron could be used to determine elegantly and conclusively how a change in a channel's biophysical properties, due to kinase action, might modulate the encoding properties of the cell. Another possibility would be to include either a Ca^{++} channel or a Ca-activated K^{+} channel in the artificial neuron to isolate the contribution of this current to the burst activity of neurons. Finally, expression of ligand-gated channels and receptors might provide the opportunity to study the phenomenon of postsynaptic integration.

References

Andersen, P., M. Raastad, and J. F. Storm (1990). Excitatory synaptic integration in hippocampal pyramids and dentate granule cells. Cold Spring Harbor Symp. Quan. Biol. 55, 81-86.

Angelotti, T.P., M.D. Uhler, and R. L. Macdonald (1993) Assembly of $GABA_A$ receptor subunits: analysis of transient single cell expression utilizing a fluorescent substrate/marker gene combination. in press.

Augustine, G. J. (1990) Regulation of transmitter release at the giant squid synapse by presynaptic delayed rectifier potassium current. J. Physiol. 31:33-364.

Auld, V., A. L. Goldin, D. S. Krafte, J. Marshall, J. M. Dunn, W. A. Catterall, N. Davidson, H. A. Lester, and R. J. Dunn (1988) A rat brain Na channel a subunit with novel gating properties. Neuron 1:449-461.

Auld, V. J., A. L. Goldin, D. S. Krafte, J. Marshall, J. M. Dunn, W. A. Catterall, H. A. Lester, N. Davidson, and R. J. Dunn (1990) A neutral amino acid change in segment IIS4 dramatically alters the gating properties of the voltage-dependent sodium channel. Proc. Natl. Acad. Sci. USA 87:323-327.

Belluzzi, O., O. Sacchi, and E. Wanke (1985) Identification of delayed potassium and calcium currents in the rat sympathetic neuron under voltage clamp. J. Physiol. 358:109-129.

Blanton, M. G., J. J. Loturco, and A. R. Kriegstein (1989) Whole cell recording from neurons in slices of reptilian and mammalian cerebral cortex. J. Neurosci. 30:203-210.

Chandler, W. K., and H. Meves (1970a) Sodium and potassium currents in squid axons perfused with flouride solution. J. Physiol. 211:623-652.

Chandler, W. K. and H. Meves (1970b) Evidence for two types of sodium conductance in axons perfused with sodium flouride solution. J. Physiol. 211:653-678.

Chandler, W. K., and H. Meves (1970c) Rate constants associated with changes in sodium conductance in axons perfused with sodium flouride solution. J. Physiol. 211:679-705.

Chandler, W. K., and H. Meves (1970d) Slow changes in membrane permeability and long-lasting action potentials in axons perfused with flouride solutions. J. Physiol. 211:707-728.

Connor, J. A. and C. F. Stevens (1971a) Inward and delayed outward membrane currents in isolated neural somata under voltage clamp. J. Physiol. 213:1-19.

Connor, J. A. and C. F. Stevens (1971b) Voltage clamp studies of a transient outward membrane current in gastropod neural somata. J. Physiol. 213:21-30.

Connor, J. A. and C. F. Stevens (1971c). Prediction of repetitive firing behavior from voltage clamp data on an isolated neuron soma. J. Physiol. 213:31-53.

Dudek, F. E., S. A. Deadwyler, C. W. Cotman, and G. Lynch (1976). Intracellular responses from granule cell layer in slices of rat hippocampus: Perforant path synapse. J. Neurophysiol. 39: 384-393.

Edwards, F. A., A. Konnerth, B. Sakmann, and T. Takahashi (1989). A thin slice preparation for patch clamp recordings from neurons of the mammalian central nervous system. Pflugers Arch. 414:600-612.

Elroy-Stein, O., T. R. Fuerst, and B. Moss (1989) Cap-independent translation of mRNA conferred by encephalomyocarditis virus 5' sequence improves the performance of the vaccinia virus/bacteriophage T7 hybrid expression system. Proc. Natl. Acad. Sci. USA 86:6126-6130.

Fournier, E. and F. Crepel (1984). Electrophysiological properties of dentate granule cells in mouse hippocampal slices maintained in vitro. Brain Res. 311: 75-86.

Fuerst, T. R., E. G. Niles, W. Studier, and B. Moss (1986). Eukaryotic transient-expression system based on recombinant vaccinia virus that synthesizes bacteriophage T7 RNA polymerase. Proc. Natl. Acad. Sci. USA 83, 8122-8126.

Grant, A. O., and C. F. Starmer (1987) Mechanisms of closure of cardiac sodium channels in rabbit ventricular myocytes: single channel analysis. Circ. Res. 60:897-913.

Hille, B. (1991) In Ionic Channels in Excitable Membranes, 2nd ed., Sinauer, Sunderland, MA.

Hines, M. (1989) A program for simulation of nerve equations with branching geometry Int. J. Biomed. Comput. 24:55-68.

Hodgkin, A. L. and A. F. Huxley (1952) A quantitative description of membrane current and its application to conduction and excitation in nerve. J. Physiol. (Lond.) 117:500-544.

Hoshi, T., W. N. Zagotta, and R. W. Aldrich (1991) 2 types of inactivation in Shaker K^+ channels--effects of alterations. Neuron 7:547-556.

Iverson, L., M. A. Tanouye, H. A. Lester, N. Davidson, B. Rudy (1988) A-type potassium channels expressed from Shaker locus cDNA. Proc. Natl. Acad. Sci. USA 85:5723-5727.

Iverson, L. E., and B. Rudy (1990) The role of the divergent amino and carboxyl domains on the inactivation properties of potassium channels derived from the Shaker gene of *Drosophila*. J. Neurosci. 10:2903-2916.

Johansson, S., W. Friedman, and P. Arhem (1992a). Impulses and resting membrane properties of small cultured rat hippocampal neurons. J. Physiol. 445: 129-140.

Johansson, S. and P. Arhem (1992b). Membrane currents in small cultured rat hippocampal neurons: a voltage-clamp study. J. Physiol. 445: 141-156.

Johansson, S. and P. Arhem (1992c). Computed potential responses of small cultured rat hippocampal neurons. J. Physiol. 445: 157-167.

Kaang, B. K., Pl J. Pfaffinger, S. G. N. Grant, E. R. Kandel, and Y. Furukawa (1992). Overexpression of an *Aplysia* Shaker K^+ channel gene modifies the electrical properties and synaptic efficacy of identified *Aplysia* neurons. Proc. Natl. Acad. Sci. USA 89:1133-1137.

Kamb, A., L. E. Iverson, and M. A. Tanouye (1987) Molecular characterization of Shaker, a Drosophila gene that encodes a potassium channel. Cell 50:405-413.

Karschin, A., B. Y. Ho, C. Labarca, O. Elroy-Stein, B. Moss, N. Davidson, and H. A. Lester (1990) Coupling of vaccinia virus expressed 5-HT_{1a} receptors to an endogenous K^+ channel in rat atrial cells. Soc. Neurosci. Abstr. 16:1123.

Karschin, A., J. Aiyar, A. Gouin, N. Davidson, and H. A. Lester (1991a) K^+ channel expression in primary cell cultures mediated by vaccinia virus. FEBS Lett. 278:229-233.

Karschin, A., B. Ho, C. Labarca, O. Elroy-Stein, B. Moss, N. Davidson, and H. A. Lester (1991b) Heterologously expressed serotonin 1A receptors couple to muscarinic K^+ channels in heart. Proc. Natl. Acad. Sci. USA 88:5694-5698.

Klaiber, K., N. Williams, T. M. Roberts, D. M. Papazian, L. Y. Jan, and C. Miller (1990) Functional expression of Shaker K^+ channels in a baculovirus-infected insect cell line. Neuron 5:221-226.

Klein, M., J. Camardo, and E. R. Kandel (1982) Serotonin modulates a specific potassium current in the sensory neurons that show presynaptic facilitation in Aplysia. Proc. Natl. Acad. Sci. USA 79:5713-5717.

Krafte, D. A., T. P. Snutch, J. P. Leonard, N. Davidson, and H. A. Lester (1988) Evidence for the involvement of more than one mRNA species in controlling the inactivation process of rat and rabbit brain Na channels expressed in Xenopus oocytes. J. Neurosci. 8:2859-2868.

Krafte, D. S., A. L. Goldin, V. J. Auld, R. J. Dunn, N. Davidson, and H. A. Lester (1990) Inactivation of cloned Na channels expressed in Xenopus oocytes. J. Gen. Physiol. 96:689-706.

Leonard, R. J., A. Karschin, J. Aiyar, N. Davidson, M. A. Tanouye, L. Thomas, G. Thomas, and H. A. Lester (1989) Expression of Shaker potassium channels in mammalian cells using recombinant vaccinia virus. Proc. Natl. Acad. Sci. USA 86:7629 -7633.

Llinas, R. (1988) The intrinsic electrophysiological properties of mammalian neurons: insights into central nervous system function. Science 242 1654-1664.

MacVicar, B. A. and F. E. Dudek (1982). Electrotonic coupling between granule cells of rat dentate gyrus: Physiological and anatomical evidence. J. Neurophysiol. 47: 579-592.

Marom, S., S. A. N. Goldsein, J. Kapper, and I. Levitan (1992). Mechanism and modulation of inactivation of the Kv3 potassium channel. Receptors and Channels In press.

Matteson, D. R., and C. M. Armstrong (1982) Evidence for a population of sleepy sodium channels in squid axons at low temperatures. J Gen. Physiol. 79:739-758.

Moorman, J. R., G. E. Kirsch, A. M. J. VanDongen, R. H. Joho, and A. M. Brown (1990) Fast and slow gating of sodium channels encoded by a single mRNA. Neuron 4:243-252.

Moss, B. (1985) in Virology, ed. Fields, B. N. (Raven, New York), pp685-703.

Moss, B and C. Fexner (1987). Vaccinia virus expression vectors. Ann. Rev. Immunol. 5: 305-324.

Patlak, J., and M. Ortiz (1985) Slow currents through single sodium channels of the adult rat heart. J. Gen. Physiol. 86:89-104.

Rettig, J., F. Wunder, M. Stocker, R. Lichtinghagen, F. Mastiaux, S. Beckh, W. Kues, P Pedarzani, K. H. Schroter, J. P. Ruppersberg, R. Veh, and O. Pongs (1992). Characterization of a Shaw-related potassium channel family in rat brain. EMBO J. 11: 2473-2486.

Patlak, J., and M. Ortiz (1986) Two modes of gating during late Na^+ channel currents in frog sartorius muscle. J. Gen. Physiol. 87:305-326.

Roberds, S. L., and M. M. Tamkun (1991). Cloning and tissue-specific expression of five voltage-gated potassium channel cDNAs expressed in rat heart. Proc. Natl. Acad.Sci. 88: 1798-1802.

Rudy, B. (1978) Slow inactivation of the sodium conductance in squid giant axons. Pronase resistance. J. Physiol. 283:1-21.

Rudy, B. (1988) Diversity and ubiquity of K channels. Neuroscience 25:729-749.

Sheng, M., M-L Tsaur, Y. N. Jan, and L. Y. Jan (1992). Subcellular segregation of two A-type K^+ channel proteins in rat central neurons. Neuron 9: 271-284.

Smith, G. L. and B. Moss (1983). Infectious poxvirus vectors have capacity for at least 25 kb pairs of foreign DNA. Gene 25:21

Stephens, E. B., R. W. Compans, P. Earl, and B. Moss (1986) Surface expression of viral proteins is polarized in epithelial cells infected with recombinant vaccinia viral vectors. EMBO J. 5:237-245.

Storm, J. F. (1988). Temporal integration by a slowly inactivating K+ current in hippocampal neurons. Nature 336, 379-381.

Stuhmer, W., C. Methfessel, B. Sakmann, M. Noda, and S. Numa (1987). Patch clamp characterization of sodium channels expressed from rat brain cDNA. Eur. Biophys. J. 14: 131-138.

Surmeier, D. J., J. Bargas and S. T. Kitai (1989). Two types of A-current differing in voltage-dependence are expressed by neurons of the rat neostriatum. Neurosci. Lett. 103: 331-337.

Timpe, L. C., T. L. Schwarz, B. L. Tempel, D. M. Papazian, Y. N. Jan, and L. Y. Jan (1988) Expression of functional potassium channels from Shaker cDNA in Xenopus oocytes. Nature 331:143-145.

Tseng-Crank, J. L., G. N. Tseng, A. Schwartz, and M. A. Tanouye (1990). Molecular-cloning and functional expression of a potassium channel cDNA from a rat cardiac library. FEBS Lett. 268, 63-68.

Yang, X.-c., C. Labarca, J. Nargeot, B. Ho, N. Davidson, and H. A. Lester (1992) Cell-specific posttranslational events affect functional expression at the plasma

membrane but not Tetrodotoxin sensitivity of the rat brain IIA sodium channel a subunit expressed in mammalian cells. J. Neurosci. 12:268-277.

Zhou, J., J. F. Potts, J. S. Trimmer, W. S. Agnew, and F. J. Sigworth (1991). Multiple gating modes and the effect of modulating factors on the μI sodium channel. Neuron 7:775-785.

Appendix 1. LacZ Staining Protocol

Wash cells w/ PBS, 1x

Fix cells w/ 0.5 ml per 35mm dish of 10% formaldehyde(37% w/w) in PBS

Incubate for 10-15 min at RT

Remove formaldehyde; wash cells w/ PBS, 1x

Stain for LacZ w/ 0.5 ml per 35mm dish of LacZ staining solution,

Incubate 2-3 hrs at 37°C

Solutions:

X-gal stock: dissolve X-gal in Dimethyleformamide at 40 mg/ml (Ref: Maniatis B14); stored at -20°C and wrapped in aluminum foil.

Staining Buffer: 5 mM potassium ferricyanide, 5 mM potassium ferrocyanide, 2 mM $MgCl_2$ stored at -4°C (Ref: J.R. Sanas, EMBO J. 5, 3133)

LacZ staining solution: 25 µl/ml of X-gal stock in staining buffer, freshly made